AD_____

Award Number: DAMD17-00-1-0467

TITLE: The Molecular Basis of Double-Strand DNA Break Repair: The Critical Structure of the RAD52/RPA Complex

PRINCIPAL INVESTIGATOR: Dobra D. Jackson
Gloria Borgstahl, Ph.D.

CONTRACTING ORGANIZATION: The University of Toledo
Toledo, Ohio 43606-3390

REPORT DATE: July 2001

TYPE OF REPORT: Annual Summary

PREPARED FOR: U.S. Army Medical Research and Materiel Command
Fort Detrick, Maryland 21702-5012

REPORT DOCUMENTATION PAGE

Form Approved
OMB No. 074-0188

1. AGENCY USE ONLY (Leave blank)	2. REPORT DATE	3. REPORT TYPE AND DATES COVERED
	July 2001	Annual Summary (15 Jun 00 - 14 Jul 01)

4. TITLE AND SUBTITLE
The Molecular Basis of Double-Strand DNA Break Repair: The Critical Structure of the RAD52/RPA Complex

5. FUNDING NUMBERS
DAMD17-00-1-0467

6. AUTHOR(S)
Dobra D. Jackson
Gloria Borgstahl, Ph.D.

7. PERFORMING ORGANIZATION NAME(S) AND ADDRESS(ES)
The University of Toledo
Toledo, Ohio 43606-3390
E-Mail: djackso2@uoft02.utoledo.edu

8. PERFORMING ORGANIZATION REPORT NUMBER

9. SPONSORING / MONITORING AGENCY NAME(S) AND ADDRESS(ES)
U.S. Army Medical Research and Materiel Command
Fort Detrick, Maryland 21702-5012

10. SPONSORING / MONITORING AGENCY REPORT NUMBER

11. SUPPLEMENTARY NOTES

12a. DISTRIBUTION / AVAILABILITY STATEMENT
Approved for Public Release; Distribution Unlimited

12b. DISTRIBUTION CODE

13. ABSTRACT ***(Maximum 200 Words)***
See next page

14. SUBJECT TERMS

15. NUMBER OF PAGES
26

16. PRICE CODE

17. SECURITY CLASSIFICATION OF REPORT	18. SECURITY CLASSIFICATION OF THIS PAGE	19. SECURITY CLASSIFICATION OF ABSTRACT	20. LIMITATION OF ABSTRACT
Unclassified	Unclassified	Unclassified	Unlimited

Understanding DNA metabolism such as DNA repair and recombination-based repair is of central importance if we are to tackle the task of finding treatments and cures for breast cancer.

Key research accomplishments are listed:

We have completely characterized the regions Rad52 binds RPA and have tested the effect of ssDNA on the interaction. Data not presented are the enhancement on DNA binding (using GMSA as collaboration, M.S.Wold laboratory) upon Rad52 binding to RPA and the electrostatic potential of the binding surfaces of Rad52 and RPA. Much has been learned about Rad52/RPA interaction and we are in the process of preparing the manuscript for publication.

We have designed a peptide with the C-terminal portion of Rad52 that has similar RPA binding activity to wt Rad52. In the contrary, our mutant Rad52 has similar aggregation properties as the wt Rad52. The solubility has greatly improved by uses of many detergents such as n-hexylglucopyranoside, which has allowed us to monitor the crystallizability of the protein with dynamic and static light scattering. The purification of the Rad52 (218-418) has been improved by adding a HQ column at high pH. We have been able to size the particles of Rad52 (218-418)thio6Xhis to be averaged from 2-4 subunits. Accomplishments for this specific aim is still ongoing.

At present we have not found conditions in which the complex of Rad52/RPA grows crystals. Hampton research screens, two dimensional grid screens and factorial screens have not yielded any hits for the Rad52/RPA mutant complex. In specific aim 1, we have localized the specific regions fully and have narrowed down the RPA binding region to the C-terminus (last 49 amino acids) and the RPA binding domain of Rad52 to be between 250-280 (30 amino acids). We are designing new constructs smaller, which will mimic the Rad52/RPA interaction surface.

We have completed specific aim 1 and preparing the manuscript for publication. Specific aim 2 has been completed and our mutant of Rad52 and RPA mimic the wt proteins in binding activities. New constructs are being prepared currently for both Rad52 and RPA. The solubility, activity, size and crystallizability will be tested upon purification of the mutant constructs.

Table of Contents

Page Number

Cover page i

Standard form 298 1

Table of Contents 2

Introduction 3

Body 3

Key Research accomplishments 9

Reportable outcomes 9-10

Conclusions 10

Appendices 11

Ranatunga W., Jackson D., Lloyd J., Forget A., Knight K., Borgstahl G., *Human Rad52 exhibits two modes of self association*, J. Biol. Chem. (2001) 276(19), p15876

Ranatunga W., Jackson D., Flowers R., Borgstahl G., *Human Rad52 has high thermal stability*, (manuscript has been accepted by Biochemistry on 4/27/01)

Table of mutants used

Introduction

Understanding DNA metabolism such as DNA repair and recombination-based repair is of central importance if we are to tackle the task of finding treatments and cures for breast cancer. Rad52 has specific interactions with RAD51, RPA and DNA (1,2,3). The binding of RAD52 to ends of double-strand breaks has been found to be a key initiation step to DNA repair by homologous recombination. RAD52 also has a self-association domain and it has been shown by EM to self-associate in solution to form ring structures (4,5). RPA is involved in many DNA metabolic processes including replication, repair, transcription and recombination. It consist of a 14, 32 and a 70 subunit which associates together to form a heterotrimer (6,7). The purpose of this research is to understand how RAD52 and RPA interact with each other at the molecular level. The crystallization of the RPA 14/32-RAD52 (221-418) complex and a three dimensional structural view of these two proteins will elucidate how these proteins are interacting. A three-dimensional structure of the RPA/RAD52 complex will reveal in depth structural knowledge of protein-protein contact surfaces, side chain interactions and binding sites for other interacting proteins. This will serve as a model for other proteins interacting with RPA 32 (such as XPA, uracil DNA glycosylase) and RAD52 (221-418) (such as RAD51). A model of the protein interactions will greatly contribute to our basic understanding of DNA repair by homologous recombination and will lead closer to future prevention, therapy and treatment of breast cancer.

Research Body

The results presented are in the order of the specific aims in the approved statement of work.

Specific aim 1- Characterize the regions of binding of RPA and Rad52 completely.

The region RPA binds Rad52 and Rad52 binding to RPA were fully defined during the first year of this report. The characterization of RPA/Rad52 binding sites were done using the modified elisa protocol, immunoprecipitation of the complexes, dynamic and static light scattering of RPA/Rad52 mutants. Also the DNA binding ability was also investigated by immunoprecipitated solution complexes (discussed in the original proposal) and gel mobility shift assays in collaboration with Dr Marc wold (sent letter of collaboration for this project). The gel mobility shift assays will not be discussed here.

Characterization of the RPA & Rad52 binding surfaces

Protein-protein interactions play an important role in Rad52-mediated double-strand break repair (1,2). This specific aim is set out to characterize the binding surfaces on both RPA and Rad52. The Rad52 binding surface for RPA (both 32 and 70 subunits) was investigated using the mutants of Rad52 shown in table 1. The technique used was a modified elisa protocol (discussed in the background section of the proposal but briefly described here. First Rad52 (1-418) and deleted constructs of Rad52 were coated to a polystyrene elisa plate and excess sites were blocked using 5% milk. Thus varying concentrations of RPA heterotrimer was added to the Rad52 bound polystyrene surface. Binding takes place in phosphate-buffer saline (150 mM salt conditions). Thus unbound RPA is washed away from the surface and the complex is probed with anti-RPA 70 or anti-RPA 32 subunit antibodies (Oncogene). These antibodies have a surface on RPA that is away from and does not interfere with the binding surface of RPA. The anti-RPA antibody is detected using a secondary HRP coupled antibody, which allows columetric detection with ABTS. Preliminary trials found that the Rad52/RPA interaction is inhibited at high salt >500mM and optimum at low to medium salt 150mM or less (data not shown). In figure 1a, we investigated whether Rad52 (218-418) can bind to RPA in comparison to the wild type Rad52 and Rad52 (1-192). The *Rad52 mutant elisa data shows the Rad52 (218-418) binds significantly to RPA heterotrimer and Rad52 (1-192) has no significant interaction with RPA heterotrimer (see figure 1).* Thus the sites allowed for RPA binding on wt Rad52 are preserved on the C-terminal fragment of Rad52. In figure 1b & c, we investigated the interaction on the 70 kDa using a variety of deletion constructs. Since the C-terminal portion of RPA 70 subunit is required for interactions with the 32 and 14 subunit (8,9), constructs with C-terminal deletions do not contain the 32 and 14 subunits however N-terminal deletions of the 70 kDa subunit contain the intact heterotrimer context. In figure 1b, C-terminal peptide fragments RPA 70^C326 and RPA 70^C442 poses a significant interaction with Rad52 (1-418) however,

RPA 70^168 doesn't interact above BSA. This maps a region of RPA 70 subunit between 168 and 326 amino acid residues. In figure 1c, the deletion constructs contain the intact heterotrimer but have

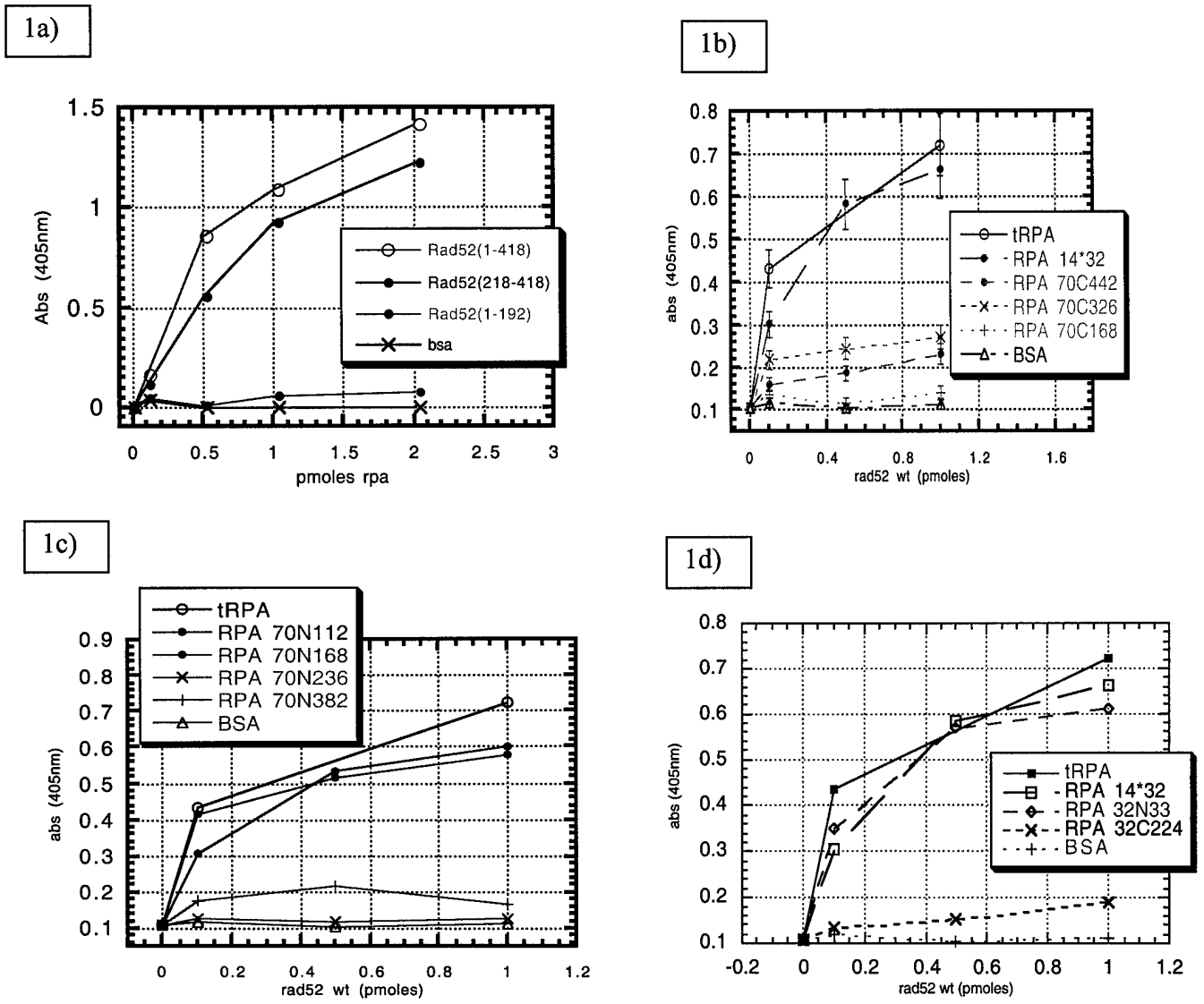

Figure 1: Rad52 and RPA complex formation detected using a modified elisa protocol. (1a) Detection of immobilized wt Rad52 and deletion mutants of Rad52 in complex with RPA heterotrimer. (1b-d) Detection of immobilized RPA and mutant RPA's with wild-type Rad52 (Rad52 (1-418)). Figure 1b contains RPA heterotrimer, RPA 14*32 heterodimer and C-terminal deletion mutant peptides of the 70 kDa subunit. Figure 1c contains heterotrimer and n-terminal deletions of the 70 kDa subunit. Figure 1d contains heterotrimer, RPA 14*32 heterodimer and deletion mutants of the 32 kDa subunit.

N-terminal deletions of the 70 kDa subunit. This figure shows that deletion mutants of the N-terminus up to 168 residues do not significantly affect the interaction with wt Rad52. Deletions beyond 168 residues of the 70 kDa subunit show a significant affect on the interaction with Rad52. Thus RPA 70^N236 and RPA 70^N382 have a significantly reduction in its interaction with Rad52 although they contain the 32 kDa subunit. In figure 1d, Deletions of the 32 kDa subunit were investigated. Thus RPA 32^N33 which is missing the N-terminal amino acids of the 32 kDa subunit doesn't have a significant interaction with Rad52. RPA 32^C224 which contains the intact heterotrimer but is missing the last 49 amino acids of the 32 kDa subunit has a significantly reduced affinity for wt Rad52. Another result found from this study is that RPA that is mutated on the N-terminus of the 32 kDa subunit to contain aspartates instead of serines to mimic phosphorylated RPA has no detectable difference in its complex forming ability with wt Rad52 (data not shown). Phosphorylation of RPA at the N-terminus is known to occur in response to DNA damage *in vivo* ().

Investigation of Rad52 binding with ssDNA bound RPA

RPA is known to undergo a significant conformational change upon binding ssDNA (). The conformational change involves changing from a globular compact upon binding short oligonucleotides (8-10 nucleotides) to an elongated extended form upon binding longer oligonucleotides (>20 nucleotides). Since Rad52 binds to a region of RPA 70 kDa subunit that is known to bind ssDNA, we investigated the complex formation with Rad52 with/ without ssDNA. For this study we immunoprecipitated the Rad52/RPA complex with an antibody –Rad52 antibody because (1) RPA binding to ssDNA requires excess ssDNA for maximum formation of the complex (10) and;(2) ssDNA can bind to elisa plates and cause high background binding of Rad52. We also confirmed the weaker 70 kDa interaction with Rad52 by using the RPA 32^C224 deletion mutant which interacted weakly on elisa plates. For this study, first, RPA was bound to oligonucleotides dT-25 and dC-8 for 30 minutes at room temperature in a buffer containing 5mM Mg^{+2} and an equal molar concentration of dT-25 and dC-8. Control samples of RPA without ssDNA were treated the same. Samples of

Figure 2: Analysis of immunoprecipitated RPA/Rad52 complex formed in the presence of short oligonucleotides poly dT-25 (dT-25) and poly dC-8 (dC-8). The complexes were set up as follows: First, equal moles of RPA and oligonucleotides were incubated in HM buffer [30mM HEPES pH=7.8, 5% inositol, ,01% np-40, 1mM DTT, 5mM $MgCl_2$] at room temperature for 30 minutes. Then equal molar concentration of Rad52 was added in HM buffer and incubated at room temperature for 1 hour. The complex was immunoprecipitated using an anti-Rad52 antibody mapped to interact with Rad52 within a region the C-terminal region (330-418).

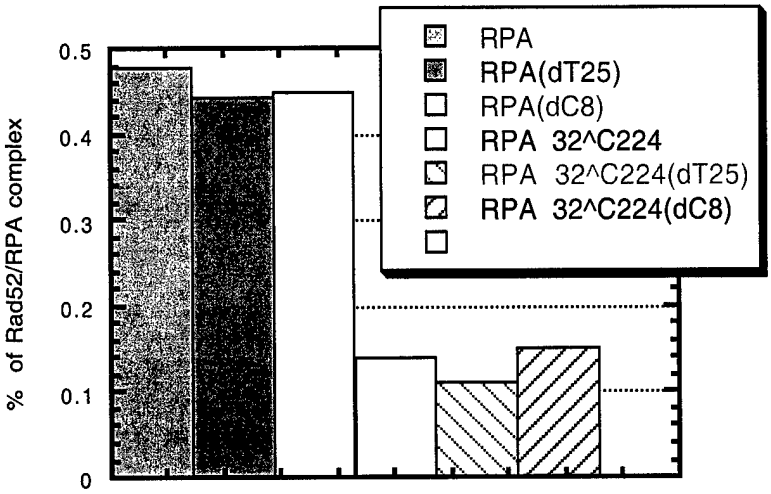

RPA and complexed RPA were added in equal molar to Rad52 (1-418). The RPA 32 kDa subunit interaction was mapped to the C-terminal region, that doesn't bind DNA and the 70 kDa subunit region is mapped to a region of RPA, which interacts strongly with ssDNA. We used the RPA 32^C224 mutant to find the effect of ssDNA bound RPA binding to Rad52. The RPA and RPA 32^224 complex interacted significantly in the immunoprecipitated complex in both the presence and absence of oligonucleotides dT-25 and dC-8. Several anti-Rad52 antibodies were developed with recognition sites in each domain of Rad52. The presence of the C-terminal site of the antibody does not interfere with the 70 kDa interaction with RPA or RPA 32^C224. Our results show that even though the 70 kDa interaction is within a site that interacts strongly with ssDNA, there is no detectable affect of the presence of ssDNA bound RPA interaction with Rad52. This indicates the 70 kDa site of interaction may lie outside the region in which RPA binds ssDNA. Also, the conformation of RPA when bound to dC-8 and dT-25 is expected to be globular and extended. No detectable effect of the length of the ssDNA is seen on its interaction with Rad52.

Specific aim 2- Develop a soluble active complex that will mimic RPA, Rad52 interaction for the purpose of crystallization.

The focus of this specific aim is to develop a soluble complex of mutants of Rad52/RPA that was active and suitable for crystallization. In our original research proposal we proposed the RPA 14*32 heterodimer and Rad52 (218-418) complex for crystallization. Preliminary results have shown that RPA 14*32 heterodimer is a suitable mutant of RPA for crystallization and our laboratory have previously established several crystal forms of the RPA 14*32 heterodimer. Here I will present the development of the C-terminal construct of Rad52 fused to a thioredoxin and a 6X polyhistidine tag. Dynamic and static light scattering tested the construct and its complex with RPA 14*32 heterodimer and RPA heterotrimer. Solution conditions were

developed for the Rad52 (218-418)thioredoxin-6X polyhistidine (called Rad52 (218-418)thio6Xhis or Rad52 (218-418) for this discussion) fusion protein.

Construction of a C-terminal fragment of Rad52 that contains the surface residues for RPA binding and contains RPA binding activity.

Results from specific aim 1 show the formation of the RPA/Rad52 complex has multiple sites for its interaction. Both on the 70 and 32 kDa subunit, are surfaces for Rad52 binding. The RPA 32 kDa subunit binding domain of Rad52 has been well established with our work and in the literature (3). However localizing the surface in which Rad52 interacts with the 70 kDa domain has been difficult. The limitation of our elisa binding is that it is difficult to detect weak interactions and their significance when using proteins with deletions in their structure. This is possibly due to slight denaturation of the protein on the polystyrene plate and different orientations of the protein when bound to the plate surface. We probed the complex in solution with various antibodies developed in our laboratory and the laboratory of Dr. Peg Wheelock and have not found a region of Rad52 that can interact significantly with the 70 kDa subunit of RPA. The best clue came from our interaction studies with Rad52 (218-418) construct. This construct contains the RPA 32 binding domain and the Rad51 binding domain of Rad52; however, it lacks the DNA binding domain and the Rad52 binding domain required for ring structure formation. The activity of the Rad52 (218-418)thioredoxin fusion protein is similar to the wt protein and however the activity of the wild-type Rad52. The purification of this mutant protein is presented here.

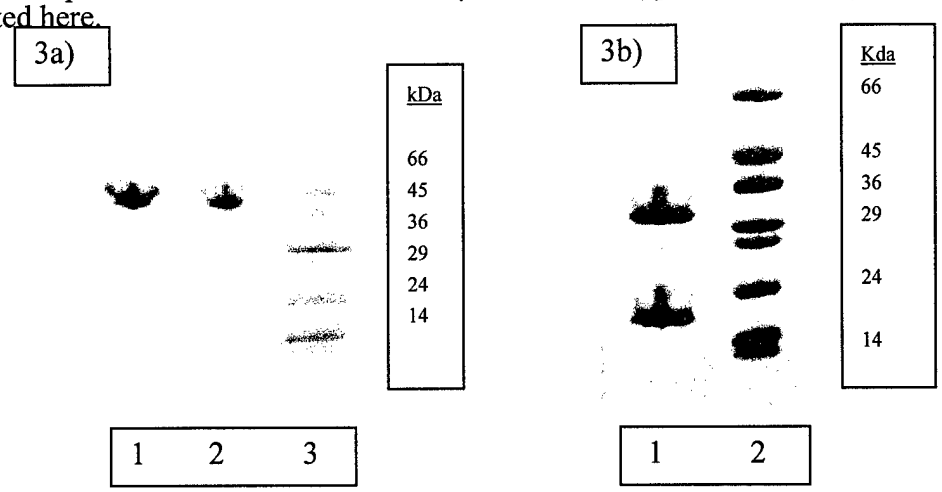

Figure 3- SDS-page purification of Rad52 (218-418) thioredoxin -poly(his)$_6$ and RPA 14*32 heterodimer. Figure 3a, lane 1 and 2 contains HQ & IMAC purified Rad52 (218-418) and figure 3b, lane 1 contains HQ purified RPA heterodimer. The purification protocol for each are published ().

In figure 3, The purification of both Rad52 (218-418) thioredoxin-poly(his)$_6$ is shown along with the SDS-page analysis of RPA 14*32 heterodimer. The purification of the RPA heterodimer is excellent and the purification of the Rad52 (218-418) thioredoxin fusion protein has much improved during the first year of this fellowship by redesigning the Rad52 (218-418) DNA expression vector and implementation of an high-Q column at high pH (i.e. pH=10.5). Thus Rad52 (218-418)thioredoxin poly(his)6 protocol has been worked out extensively and the accomplishments include: (1) we redesigned the expression vector to include a 6X polyhistidine tag along with an histidine patch thioredoxin fusion protein which was present in our purification shown in the preliminary data. We have also cloned the DNA sequence into a pET28a vector and express the fusion construct using a strong T7-promotor driven system instead of the previous arabinose driven promotor system in the pBAD vector (INVITROGEN). The pET28a vector allows for higher expression and use of codon-plus BL21(DE3) cells for better expression of sequences with rare codons in *E. coli.*

Size analysis of RPA 14*32 heterodimer and Rad52 (218-418)thioredoxin-poly(his)$_6$ complex

The size of the Rad52/RPA complex formed in solution was examined by static light scattering. This technique was developed in our lab to help in analysis of these complexes, study aggregation and crystal formation. The result of static light scattering is an average molecular weight of the protein in solution and the second virial coefficient. The second virial coefficient can be related to the ability of a protein or complex to crystallize and will be discussed in specific aim 3. Here we will only focus on the size and relate the theoretical ratio of the complex to the experimental results.

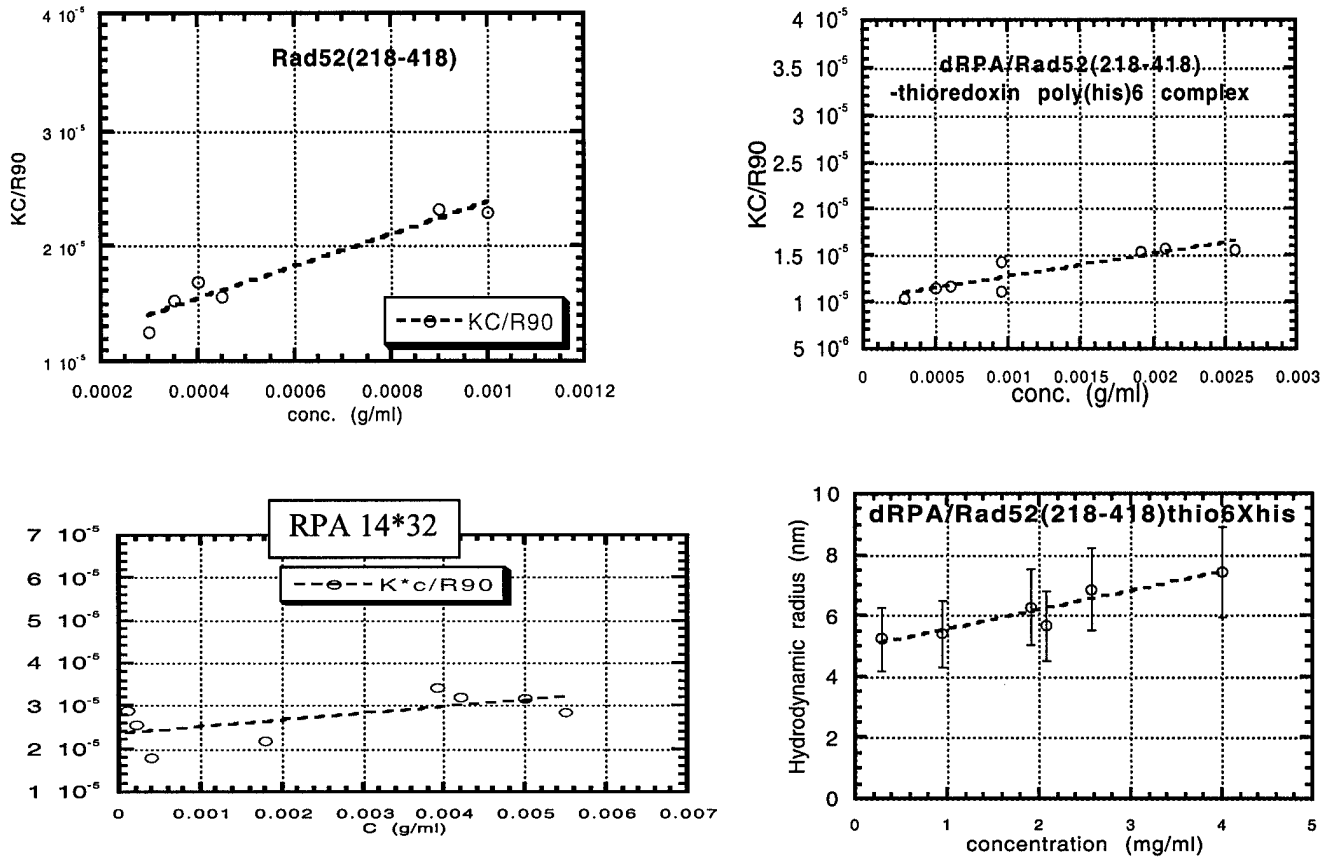

Figure 4: Total intensity light scattering of RPA 14*32, Rad52 (218-418)thio6Xhis alone and complexes. The measurements were taken using a dynamic & static light scattering instrument (Dynapro 801) developed by Protein Solutions. Time averaged total intensity was taken at 90* angles and Rayleigh ratios were calculated using the dynapro software and microsoft EXCEL. The dn/dC value used for all three proteins was .186 ml/g. Figure 4d contains the change in the average hydrodynamic radius with concentration. All concentrations were measured by the Bradford method.

The solution behavior of Rad52 (218-418)thio6Xhis was extensively studied by light scattering. We found the size of the Rad52 (218-418) fusion construct to have an average molecular weight of approximately 112 kDa with a 25 kDa error. This size makes to range between 2 and 4 particles with the average near three is consistent with electron microscopy investigations (see appendices). The molecular weight of the RPA heterodimer was measured under our conditions and found to be close to monomeric value at low concentrations. Interestingly, the Rad52 (218-418)thio6Xhis/RPA 14*32 complex was measured to have an average molecular weight of 99 kDa with a 22kDa error. The error includes errors in fluctuation of intensity measurements and errors in the measured concentrations. We also see a consistent decrease in the average hyrodynamic radius of the complex (Table 2). This implies our complex is disrupting higher order particles of Rad52 (218-418). This is also consistent with the formation of the Rad52 (218-418)thio6Xhis complex with RPA heterotrimer (data not shown).

Table 2: Values for static light scattering of Rad52 (218-418), RPA 14*32, and complexes of each

Protein	conc.	M.W.	error	Radius	error
	(mg/ml)	(kDa)	(kDa)	(nm)	(nm)
RPA 14*32	.2-4	42.3		3.27	.65

Rad52(218-418)	.2-1	102	13.2	4.9	1.5
RPA 14*32/Rad52 (218-418) complex	.2-2.5	97.1	14.1	4.24	1.1
RPA heterotrimer	.1-5	117		5.23	1.3
RPA heterotrimer / Rad52 (218-418) complex	.1-3	157		5.04	1.0

Specific aim 3- To determine solution conditions which favor the interaction between RPA and Rad52 and promote crystallization.

Solution conditions for the RPA/Rad52 fragment complex were determined by using dynamic light scattering. Significant crystallization variables were screened such as pH, concentration, detergents, mono and divalent cations, organic and additive screens (Hampton Research) were tested for improvement in solubility and measured hydrodynamic radius using dynamic light scattering.

Table 3: Dynamic light scattering of Rad52 (218-418)thio6Xhis alone and in detergents supplied by Hampton Research.

Detergent	type	CMC [mM]	[act] [mM]	R_H	C_P	C_P/R_H (%)	M.W.	Baseline	SOS
$C_{12}E_9$	N	.08	.004	.92	.7	76	2.4	1.007	5.45
Sucrose Monolaurate	N	.2	.01	5.86	3.9	67	224.5	1.012	6.52
CYMAL-6	N	.56	.028	4.63	2.4	52	119.7	1.005	20.58
ZWITTERGENT 3-12	Z	4	.2	4.65	2.5	54	120.5	1.005	20.62
LDAO	N	2	.1	4.4	2	45	105.7	1.003	15.163
n-decyl-maltoside	N	1.8	.09	4.17	1.9	46	92.3	1.002	11.715
DeoxyBigChap	N	1.4	.07	4.37	1.9	43	103.7	1.005	9.362
Nonly-glucoside	N	6.5	.325	4.65	2.5	54	121.4	1.006	20.8
DDAO	N	10.4	.52	4.4	1.9	43	104.1	1.005	8.9
HECAMEG	N	19.5	.98	4.46	2.1	47	110	1.006	9.90
n-octly-glucoside	N	24.5	1.22	4.9	2.2	45	146.1	1.002	2.4
C-HEGA-10	N	35	1.75	4.32	1.9	44	100.8	1.008	8.51
MEGA-8	N	79	3.95	4.78	2.3	48	130.6	1.001	.527
n-hexyl-glucoside	N	250	12.5	4.66	2.2	47	122.3	1.001	.685
CTAB	I	10	------	------	----	-----	------	------	-----
No detergent	---	----	-----	4.00	4.0	.99	86.9	1.022	34.99

11) For CTAB, the protein precipitated during dialysis and the baseline was too unstable to read.

12) All values entered were taken assuming a monomodal distribution.

13) The protein concentration used was 1 mg/ml.

14) For all detergents, 20-25 data points were taken and no more than 10% of the data was marked. (except for the no detergent control which only 13 data points could be collected before the program timed-out).

Dynamic light scattering analysis of Rad52(218-418)thio6Xhis/RPA complex are still ongoing. The RPA 14*32 heterodimer has been studied by dynamic light scattering and the conditions are well established for monodisperse protein. Rad52(218-418)thio6Xhis is not as well behaved in solution and is near monodispersed only at low concentrations. At concentrations required for crystallization (<5mg/ml) Rad52 (218-418)thio6Xhis aggregates in solution. Without detergent Rad52 (218-418) is completely insoluble at 4mg/ml. A significant improvement in the behavior of the Rad52 (218-418) protein came from a Hampton research detergent screen. The dynamic light scattering data for the detergent screen are shown here in table 3. Each detergent listed improved the baseline and polydispersity (in Cp/Rh) value, which demonstrates the driving force for the formation of the aggregates, is hydrophobic. In the presence of n-hexylglucopyranoside at a concentration 20-fold lower than the CMC significantly improved the monodispersity of Rad52 at 1 mg/ml. Also, Rad52 (218-418) in both constructs forms higher order particles in solutions which has been demonstrated by static light scattering (specific aim 2) in the presence of .5 mM n-hexyl-glucopyranoside. The behavior of Rad52 (218-418) in the presence of n-hexyl glucopyranoside yields a near monodisperse reading at 1 mg/ml and sizes at a protein to contain 2-4 subunits. We suspect that the intraparticle interactions in the presence of detergent are specific and Rad52 contains a separate self associating domain located at the C-terminus of the protein (see reference in appendix). The same behavior in the presence of detergents are also seen with wt Rad52 (Ranatunga, unpublished). Dynamic light scattering analysis has revealed that the key driving force for the intraparticle interactions is hydrophobic and the presence of a detergent at significantly high concentrations can break up nonspecific aggregates and increase the solubility of the protein.

Specific aim 4&5- Obtain diffraction quality crystals of the RPA, Rad52 complex and solve the crystallographic phase problem and the structure of the RPA/Rad52 complex.

Specific aim 4 is in progress and successful completion of it is required for specific aim 5. Crystallization screens from Hampton research have been attempted with no success yet with the Rad52 (218-418)thio, Rad52 (218-418)thio6Xhis, and both in complex with RPA 14*32 heterodimer. In present and future experiments include redesigning Rad52 and RPA constructs for crystallization. Enterokinase and thrombin cleavage of the thioredoxin and 6X his tag of Rad52 and RPA was found to cleave nonspecifically by mass spectroscopy and SDS page analysis. We have recently redesigned the C-terminal fragment of Rad52 to start at residue 212 (instead of 218) which is another flexible region of Rad52 structure predicted by a secondary structure analysis program. Also for this construct we omitted the thioredoxin fusion protein. Purification and analysis is ongoing and will continue for the following year.

Key research accomplishments

Key research accomplishments are listed within the specific aim:

Specific aim 1- the data for this specific aim has been completed. We have completely characterized the regions Rad52 binds RPA and have tested the effect of ssDNA on the interaction. Data not presented are the enhancement on DNA binding (using GMSA as collaboration, M.S.Wold laboratory) upon Rad52 binding to RPA and the electrostatic potential of the binding surfaces of Rad52 and RPA. Much has been learned about Rad52/RPA interaction and we are in the process of preparing the manuscript for publication.

Specific aim 2 & 3- we have designed a peptide with the C-terminal portion of Rad52 that has similar RPA binding activity to wt Rad52. In the contrary, our mutant Rad52 has similar aggregation properties as the wt Rad52. The solubility has greatly improved by uses of many detergents such as n-hexylglucopyranoside, which has allowed us to monitor the crystallizability of the protein with dynamic and static light scattering. The purification of the Rad52 (218-418) has been improved by adding a HQ column at high pH. We have been able to size the particles of Rad52 (218-418)thio6Xhis to be averaged from 2-4 subunits. Accomplishments for this specific aim is still ongoing.

Specific aim 4 & 5- At present we have not found conditions in which the complex of Rad52/RPA grows crystals. Hampton research screens, two dimensional grid screens and factorial screens have not yielded any

hits for the Rad52/RPA mutant complex. In specific aim 1, we have localized the specific regions fully and have narrowed down the RPA binding region to the C-terminus (last 49 amino acids) and the RPA binding domain of Rad52 to be between 250-280 (30 amino acids). We are designing new constructs smaller, which will mimic the Rad52/RPA interaction surface.

Reportable outcomes

The results of this research has been reported in the following literature and events:

Ranatunga W., Jackson D., Lloyd J., Forget A., Knight K., Borgstahl G., *Human Rad52 exhibits two modes of self association*, J. Biol. Chem. (2001) 276(19), p15876

Ranatunga W., Jackson D., Flowers R., Borgstahl G., *Human Rad52 has high thermal stability*, (manuscript has been accepted by Biochemistry on 4/27/01)

Presentations:

Jackson D., Borgstahl G., *Characterization of the Rad52/RPA protein-protein interaction, (presented at the Sigma Xi symposium on 5/20/01)*

Jackson D., Ranatunga W., Lloyd J., Forget A., Knight K., Borgstahl G. *The self association of the C-terminal half of human Rad52 and its interaction with human RPA* (will be presented at the 15th annual Protein Society symposium as a poster)

Conclusions

We have completed specific aim 1 and preparing the manuscript for publication. Specific aim 2 has been completed and our mutant of Rad52 and RPA mimic the wt proteins in binding activities. New constructs are being prepared currently for both Rad52 and RPA. The solubility, activity, size and crystallizability will be tested upon purification of the mutant constructs.

References

(1) Shinohara, A., Tomoko O., *Homologous recombination and roles of double-strand breaks* (1995), TIBS, 20, p387-91

(2) Shen Z., Cloud K., Chen D., Park M., *Specific interactions between the human Rad51 and Rad52 proteins*(1996), J. Biol. Chem., 271, p148-152

(3) Park M., Ludwig D., Stigger E., Lee S., *Physical interaction between human Rad52 and RPA is required for homologous recombination in mammalian cell,* (1996) J. Biol. Chem., 271, p18996

(4) Shinohara A., Shinohara M., Ohta S., Matsuda S., Ogawa T., *Rad52 forms rings structures and co-operates with RPA in single-strand annealing,* (1998) Genes to cells, 3, p145-156

(5) Van Dyck E., Nasser MA., Stasiak A., West S., *Visualization of human Rad52 protein and its complexes with Rad51 and DNA*, (1998) J. Mol. Biol., v284, p1027-38

(6) Wold M., *Replication protein A: A heterotrimeric single-stranded DNA binding protein required for eukaryotic DNA metabolism* (1997) Annu. Rev. Biochem., 66, p61-92

(7) Hendrickson L., Umbricht C., Wold M., *Recombinant Replication protein A: expression, complex formation and functional characterization*, (1994) J. Biol. Chem., v269 (15), p11121-32

(8) Braun KA., Lao Y., Zhigang H., Ingles J., Wold MS., *Role of protein-protein interactions in the function of Replication protein A (RPA): RPA modulates the activity of DNA polymerase alpha by multiple mechanisms,* Biochemistry, 36(28), p8443-8454

(9) Gomes X., Wold MS., *Functional domains of the 70-kDa subunit of human Replication Protein A,* Biochemistry, 35(32), p10558-68

(10) Changsoo K., Wold MS., *Recombinant human replication protein A binds to polynucleotides with low cooperativity*, **Biochemistry** 34, p20058

APPENDICES

Table 1: Rad52 mutants used for this research. *The Rad52 (218-418)-thioredoxin-(poly-His)$_6$ was developed during the first year of this investigation.* The other two Rad52 constructs (Rad52 1-192, Rad52 1-418 i.e. wtRad52) were gifts from Dr. Min Park at Los Alamos National Laboratories. The development of Rad52(218-418)-thioredoxin-(poly-His)$_6$ is discussed in specific aim 2.

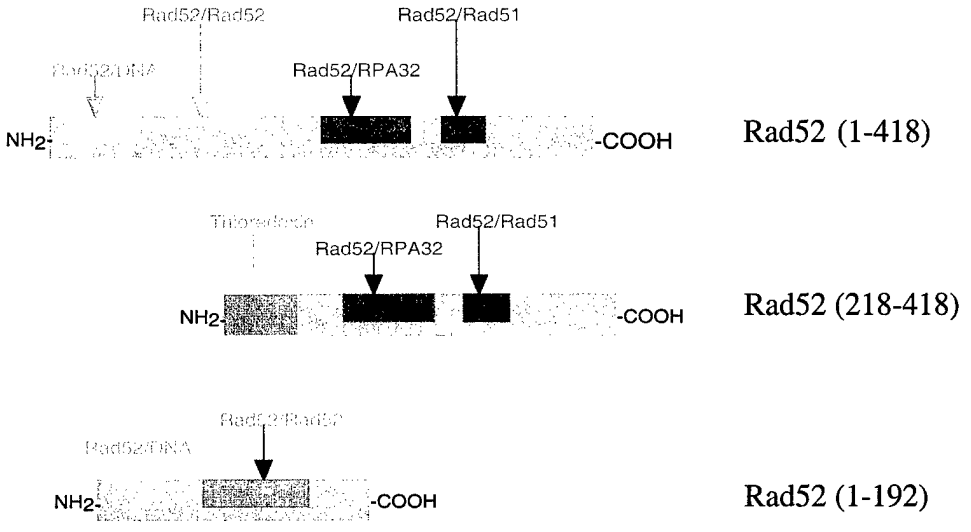

Table 2: RPA and RPA mutants used. RPA heterotrimer and mutant RPA constructs were developed by Dr. Marc Wolds lab prior to starting this research and were a kind donation to our lab and objective. The activities characterized with each construct is listed along with the nomenclature used for each mutant. Abbreviations: 70NXXX or 32NXXX is missing the XXX number of amino acids from the n-terminus of the 70 kDa subunit or 32 kDa subunit. CXXX means it is missing the residues from the c-terminus to to residue XXX. The 70 kDa subunit has 616 residues and the 32 kDa subunit has 271 residues. The 14 kDa subunit has 120 amino acid residues. Below are shown the known sites for phosphorylation of RPA 32 subunit which are mutated to aspartic acid in RPA^32asp8 mutant.

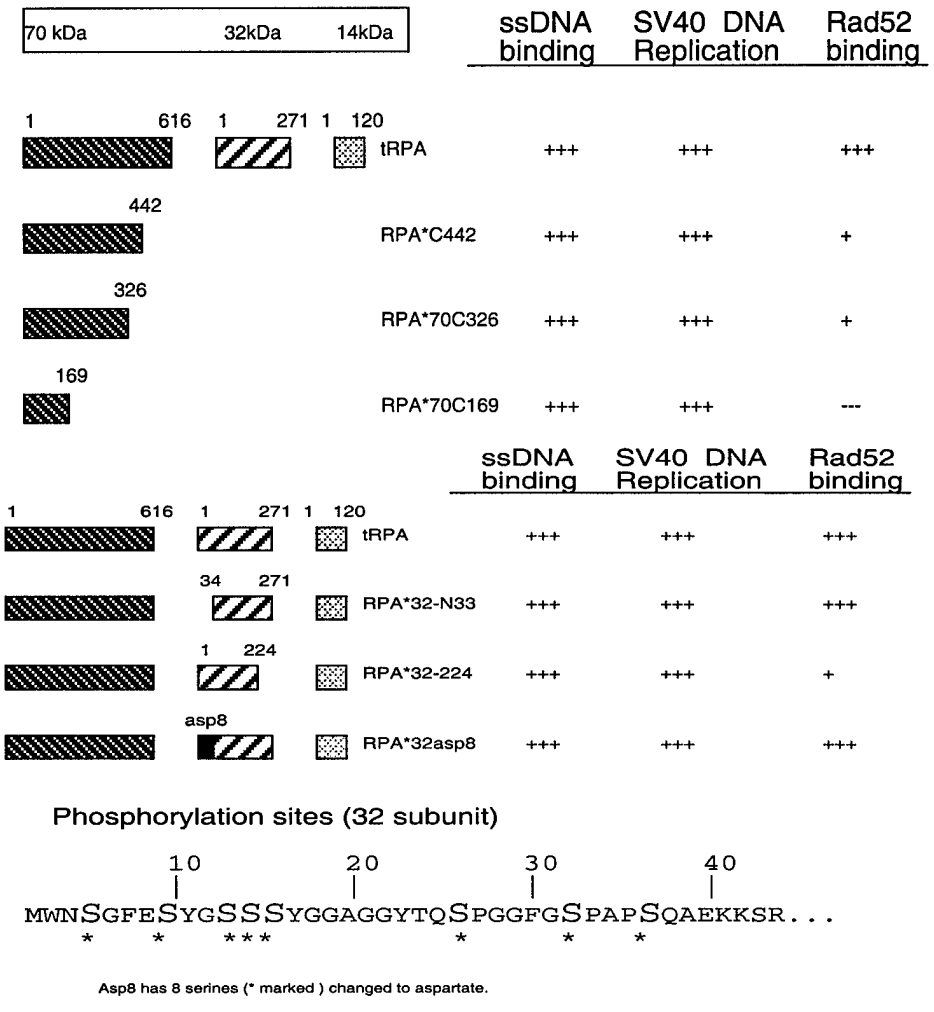

THE JOURNAL OF BIOLOGICAL CHEMISTRY
Vol. 276, No. 19, Issue of May 11, pp. 15876–15880, 2001
Printed in U.S.A.

Human RAD52 Exhibits Two Modes of Self-association*

Received for publication, December 27, 2000
Published, JBC Papers in Press, February 13, 2001, DOI 10.1074/jbc.M011747200

Wasantha Ranatunga‡§, Doba Jackson‡§, Janice A. Lloyd§¶, Anthony L. Forget§¶, Kendall L. Knight¶, and Gloria E. O. Borgstahl‡‖

From the ‡Department of Chemistry, University of Toledo, Toledo, Ohio 43606-3390 and the ¶Department of Biochemistry and Molecular Pharmacology, University of Massachusetts Medical School, Worcester, Massachusetts 01655-0103

The human RAD52 protein plays an important role in the earliest stages of chromosomal double-strand break repair via the homologous recombination pathway. Individual subunits of RAD52 self-associate into rings that can then form higher order complexes. RAD52 binds to double-strand DNA ends, and recent studies suggest that the higher order self-association of the rings promotes DNA end-joining. Earlier studies defined the self-association domain of RAD52 to a unique region in the N-terminal half of the protein. Here we show that there are in fact two experimentally separable self-association domains in RAD52. The N-terminal self-association domain mediates the assembly of monomers into rings, and the previously unidentified domain in the C-terminal half of the protein mediates higher order self-association of the rings.

The repair of double-strand breaks in chromosomal DNA is of critical importance for the maintenance of genomic integrity. In *Saccharomyces cerevisiae*, genes of the *RAD52* epistasis group, *RAD50*, *RAD51*, *RAD52*, *RAD54*, *RAD55*, *RAD57*, *RAD59*, *MRE11*, and *XRS2*, were identified initially by the sensitivity of mutants to ionizing radiation (1, 2). These genes have been implicated in an array of recombination events including mitotic and meiotic recombination as well as double-strand break repair. *RAD52* mutants show the most severe pleiotropic defects suggesting a critical role for the protein in homologous recombination and double-strand break repair (2). The importance of specific protein-protein interactions in the catalysis of homologous recombination is suggested by studies demonstrating specific contacts and functional interactions between Rad52p and a number of proteins involved in recombination including Rad51p (3–8), which catalyzes homologous pairing and strand exchange, and replication factor A (RPA)[1] (8–10), a heterotrimeric single-stranded DNA binding protein (11).

Studies of the equivalent human proteins have identified similar interactions between the RAD52, RAD51, and replication protein A proteins (12–17). Based on a series of protein-protein interaction assays (15, 16, 18) and DNA binding studies[2] (16), a domain map of RAD52 was proposed by Park *et al.* (16) (see Fig. 1). The determinants of self-association were proposed to exist exclusively within a region defined by residues 65–165, a result supported by recent studies of several isoforms of RAD52 (19). Electron microscopy (EM) studies of Rad52p and RAD52 have revealed formation of ring-shaped structures (9–13 nm in diameter), as well as higher order aggregates (9, 12, 20). Stasiak *et al.* (21) performed image analyses of negatively stained electron micrographs and determined that the 10-nm RAD52 rings are composed of seven subunits. Scanning transmission electron microscopy (STEM) analysis indicated a mean mass of 330 ± 59 kDa supporting a heptameric ring-shaped RAD52 structure (21). Recent studies show that RAD52 binds to double-stranded DNA ends as an aggregated complex (20). These end-binding complexes were amorphous in shape and ranged in size from 15 to 60 nm. Within these complexes, RAD52 rings were observed occasionally. Binding of RAD52 to the DNA ends promoted end-to-end association between DNA molecules and stimulated ligation of both cohesive and blunt DNA ends (20).

Therefore, given that the formation of both ring-shaped oligomers and aggregates of these rings seem relevant to RAD52 function, we sought to investigate further the self-association properties of the RAD52 protein. We performed a series of analyses comparing full-length RAD52-(1–418) with two different mutant RAD52 proteins: (i) a 1–192 mutant that spans the N-terminal portion and includes the entire proposed DNA binding and self-association domains and (ii) a 218–418 mutant that spans the C-terminal portion of RAD52 that includes the proposed RPA- and RAD51-binding domains (Fig. 1). In contrast to previous studies, our results show that there are experimentally separable determinants for two different modes of self-association by RAD52, one in the N-terminal and one in the C-terminal portion of the protein.

EXPERIMENTAL PROCEDURES

RAD52 Constructs—Wild-type *RAD52* and *RAD52*-(1–192) pET28 expression plasmids were a gift from Dr. M. Park and have six histidines fused to the C terminus. A pET28 expression plasmid containing the thioredoxin-RAD52-(218–418) fusion protein was constructed using standard polymerase chain reaction techniques.

Protein Purification—Cultures of transformed BL21(DE3) Codon Plus *Escherichia coli* (Stratagene) were grown in a fermentor and induced with 0.5 mM isopropyl-1-thio-β-D-galactopyranoside. Wild-type *RAD52* and *RAD52*-(1–192) cells were resuspended in a buffer consisting of 20 mM HEPES, pH 6.0, 10% glycerol, 400 mM NaCl, 100 mM KCl, 5 mM β-mercaptoethanol, 1 mM dithiothreitol, 1 mM hexylglucopyranoside, and 1 mM EDTA. *RAD52*-(218–418) cells were resuspended in a

* This work was supported by the United States Army Medical Research and Material Command under DAMD17-98-1-8251 (to G. E. O. B.) and National Institutes of Health Grant GM44772 (to K. L. K.). Brookhaven National Laboratory STEM is supported by National Institutes of Health Grant P41-RR01777 and partially supported by the Department of Energy and Office of Biological and Environmental Research. The costs of publication of this article were defrayed in part by the payment of page charges. This article must therefore be hereby marked "*advertisement*" in accordance with 18 U.S.C. Section 1734 solely to indicate this fact.

§ These authors contributed equally to this work.
‖ To whom correspondence should be addressed: Dept. of Chemistry, University of Toledo, 2801 W. Bancroft St., Toledo, OH 43606-3390. Tel.: 419-530-1501; Fax: 419-530-4033; E-mail: gborgst@uoft02.utoledo.edu.

[1] The abbreviations used are: RPA, replication protein A; MES, 4-morpholineethanesulfonic acid; EM, electron microscopy; STEM, scanning transmission electron microscopy; BSA, bovine serum albumin; DLS, dynamic light scattering.

[2] J. A. Lloyd, and K. L. Knight, unpublished data.

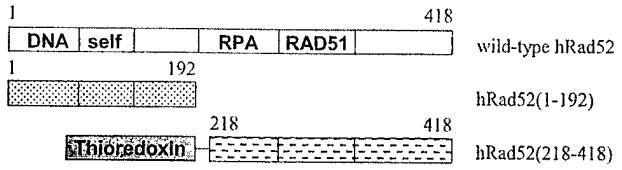

FIG. 1. **Schematic diagram of wild-type RAD52 and deletion mutants.** The beginning and ending residue numbers of each mutant are indicated along with domain structure. The following domains and residue numbers were defined by Park *et al.* (16): DNA binding, 39–80; self-association, 85–159; RPA binding, 221–280; RAD51 binding, 290–330.

buffer consisting of 50 mM HEPES, pH 8, 500 mM KCl, 500 mM $LiSO_4$, 2.5% glycerol, 1 mM EDTA, 5 mM dithiothreitol, 4 mM imidazole, and 0.1% Triton X-100. Protease inhibitors (1 mM phenylmethylsulfonyl fluoride and 10 mM benzamidine) were used throughout purification. Cells were lysed using a French press, and the lysate was clarified by centrifugation, filtration through Cell Debris Remover-modified cellulose (Whatman), and passage through a 0.22-μm pore filter. The clarified lysate was applied to an MC/M Ni^{2+} affinity column (PerSeptive Biosystems) that was optimally washed and eluted with an imidazole gradient. Wild-type RAD52 and RAD52-(1–192) then were dialyzed extensively against a buffer consisting of 20 mM MES, pH 6.0, 10% glycerol, 400 mM NaCl, 100 mM KCl, 5 mM β-mercaptoethanol, 1 mM dithiothreitol, 1 mM hexylglucopyranoside, and 1 mM EDTA. RAD52-(218–418) was dialyzed extensively against a buffer consisting of 50 mM HEPES, pH 8.0, 2.5% glycerol, 2.5 mM EDTA, and 0.5 mM hexylglucopyranoside and then purified further by anion exchange using an HQ/M column (PerSeptive Biosystems) eluted with a KCl gradient. Protein samples were concentrated using Amicon concentrators with YM10 membranes, and protein concentrations were determined using Bradford assay (Bio-Rad) with bovine serum albumin (BSA) as a standard. The expression plasmid for wild-type RPA heterotrimer was a gift from Dr. M. Wold. RPA was expressed and purified as described (22).

Enzyme-linked Immunosorbent Assay—The enzyme-linked immunosorbent assay was done at room temperature. Briefly, 10 pmol of wild-type RAD52, RAD52 mutants, or BSA were coated to microtiter plates for 1 h. Plates were washed three times with phosphate-buffered saline (PBS) containing 0.02% Tween 20 to remove unbound protein. Plates then were blocked with 5% milk in PBS for 10 min and then washed. Various amounts of RPA in PBS and 5% milk were added and incubated for 1 h. Plates then were washed to remove nonspecific interactions and probed with a monoclonal antibody against the 70-kDa subunit of RPA (Calbiochem) in PBS and 5% milk for 30 min. Plates then were washed and probed with anti-mouse IgG peroxidase conjugate (Sigma) in PBS and 5% milk for 30 min and washed. Plates were developed using 3,3′,5,5′-tetramethylbenzidine in phosphate-citrate buffer with 0.03% hydrogen peroxide. Color was developed for 30 min, the reaction was stopped with 1.5 M H_2SO_4, and absorbance readings at 450 nm were taken with a microtiter plate reader. Background absorbance was determined from a blank well and then subtracted from the data.

Gel-shift DNA Binding Assays—Reactions (20 μl) contained 20 mM triethanolamine-HCl, pH 7.5, 1 mM dithiothreitol, 1 mM $MgCl_2$, 0.1 mg/ml BSA, 0.05% Tween 20, 2 nM 5′-end-labeled 95 base oligonucleotide (concentration in bases), and the indicated amounts of protein. The oligonucleotide sequence is as follows: 5′-AGA CGA TAG CGA AGG CGT AGC AGA AAC TAA CGA AGA TTT TGG CGG TGG TCT GAA CGA CAT CTT TGA GGC GCA GAA AAT CGA GTG GCA CTA ATA AG-3′. Reactions were incubated at 37 °C for 20 min followed by the addition of glutaraldehyde to 0.2% and continued incubation at 22 °C for 20 min. Glycerol was added to a final concentration of 1.6% (w/v) and samples (10 μl) were loaded onto a 0.8% agarose gel and electrophoresed at 100 mV in 0.5× TBE buffer (90 mM Tris, 64.6 mM boric acid, and 2.5 mM EDTA, pH 8.3). Gels were analyzed using a Molecular Imager FX and QuantityOne software (Bio-Rad). The 95-base oligonucleotide used in the gel-shift assays was made using an ABI 392 DNA/RNA synthesizer.

Dynamic Light-scattering (DLS) Analysis—DLS was carried out using a DynaPro-801 molecular sizing instrument equipped with a microsampler (Protein Solutions). A 50-μl sample was passed through a filtering assembly into a 12-μl chamber quartz cuvette. For RAD52-(1–192) and RAD52-(218–418), 20-nm filters were used. For wild-type RAD52, a 100-nm filter was used. The data were analyzed first using Dynamics 4.0 software and then DynaLS software as follows. Hydrodynamic radii (R_H) for monomodal distributions, as defined by a baseline ranging from 0.977 to 1.002, were reported from Dynamics 4.0. Bi- and multimodal distributions were analyzed using DynaLS. DynaLS data estimates of molecular weight were obtained from R_H using Dynamics 3.0 molecular weight calculator. Sum of squares errors less than 5000 were considered negligible.

FIG. 2. **Negative stained electron micrograph of wild-type RAD52.** Wild-type RAD52 (4.0 μM) was prepared as described under "Experimental Procedures." Larger spherical particles are ~80 nm in diameter, half-spheres are 50 nm, and numerous 10-nm rings are visible also. *Black bar* = 0.1 μm.

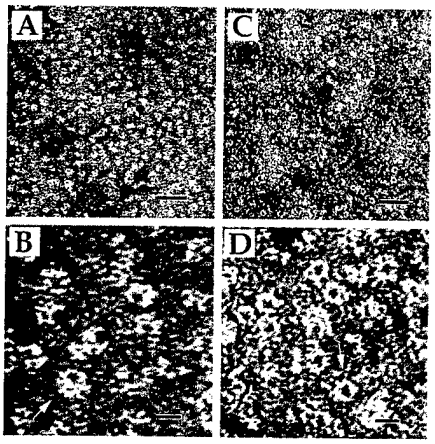

FIG. 3. **Negative stained electron micrographs of wild-type RAD52 and RAD52-(1–192) protein.** Proteins (4.0 μM) were prepared as described under "Experimental Procedures." The majority of protein for both wild-type RAD52 (*A* and *B*) and RAD52-(1–192) (*C* and *D*) forms 10-nm diameter ring-shaped oligomers. Larger particles of wild-type RAD52 in *A* (also see Fig. 2) are not formed by RAD52-(1–192). Higher magnifications of both proteins reveal that the protrusions observed on the 10-nm rings of wild-type RAD52 are missing in the RAD52-(1–192) rings (*arrows* in *B* and *D*). *Black bars* = 0.05 μm in *A* and *C* and 0.01 μm in *B* and *D*.

Electron Microscopy—Proteins were prepared for EM by diluting wild-type or mutant RAD52 to 4.0 μM in a buffer containing 20 mM Tris-HCl, pH 7.5, 5% glycerol, 5 mM β-mercaptoethanol, 0.1 mM EDTA, and 100 mM KCl. Samples were spread onto thin carbon films on holey carbon grids (400 mesh), stained with 1% uranyl acetate, and visualized by transmission electron microscopy using a Philips CM10 microscope.

STEM Analysis—Analyses were carried out at the Brookhaven National Laboratory using unstained, unshadowed freeze-dried samples. Protein samples (~0.1 mg/ml) were applied to a thin carbon film supported by a thick holey film on titanium grids and freeze-dried overnight. The microscope operates at 40 kV. Operation of the STEM and data analyses were performed as described previously (23).

Gel Filtration—Samples of the RAD52-(218–418) protein at 1.2 mg/ml were loaded onto a Superdex 200 HR 10/30 gel filtration column (Amersham Pharmacia Biotech/LKB) equilibrated in buffer containing 20 mM MES, pH 6.0, 400 mM NaCl, 100 mM KCl, 10% (w/v) glycerol, 5 mM β-mercaptoethanol, and 1 mM EDTA. Analysis was performed using a BioLogic chromatography system (Bio-Rad) with an in-line UV detector.

RESULTS

Oligomeric Characteristics of RAD52 Proteins—EM analyses of wild-type RAD52 and RAD52-(1–192) show that both proteins form ring-shaped structures (Figs. 2 and 3). The average diameter of these particles, measured across the surface with the central pore, is 10 ± 1 nm, consistent with previous reports (9, 12, 21). Wild-type RAD52 also forms distinct larger particles that appear as various sized spheres and half-spheres ranging in diameter from 30 to 100 nm (Fig. 2). These particles consist of individual 10-nm rings as well as other less distinct com-

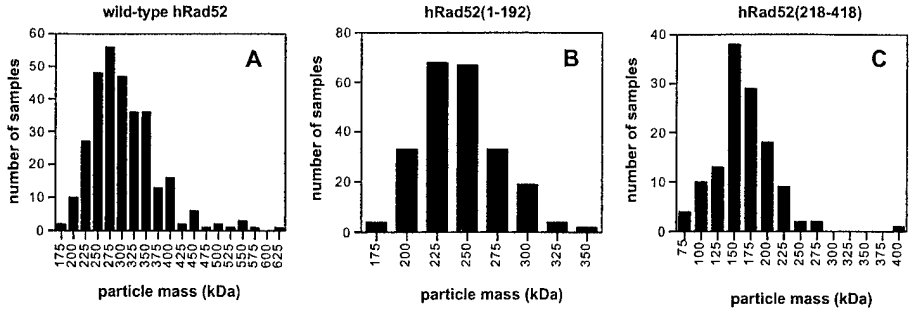

FIG. 4. **STEM histograms.** STEM mass analyses were performed as described under "Experimental Procedures." Histograms include pooled data from several separate analyses (eight for wild-type RAD52, six for RAD52-(1–192), and five for RAD52-(218–418)). Average mass values were as follows: *A*, wild-type RAD52 298 ± 69 kDa (n = 309); *B*, RAD52-(1–192) 227 ± 30 kDa (n = 277); *C*, RAD52-(218–418) 153 ± 40 kDa (n = 119).

TABLE I
Dynamic light-scattering measurements of RAD52 proteins

Protein	Concentration	Base line	Modality	SOS[a]	R_H[b]	Molecular mass	Peak[c] area
	mg/ml			*error*	*nm*	*kDa*	*%*
RAD52	3.5	1.007	Multimodal	3.10	6.6 (0.7)	279	10.5
					27.6 (9.3)	9.05×10^3	85.8
					711.0 (245)	2.40×10^7	3.7
RAD52-(1–192)	15	1.001	Monomodal	1.95	5.7 (1.2)	200	
RAD52-(218–418)	2	1.001	Monomodal	0.64	4.6 (2.1)	118	
Thioredoxin	1	1.001	Monomodal	3.3	2.0 (0.8)	14.8	

[a] SOS, sum of squares.
[b] Average hydrodynamic radius (R_H) is reported with the polydispersity (width of the distribution in nm) given in parentheses.
[c] For DynaLS results the percent peak area for the solvent peak is not reported.

pressed structures. For RAD52-(1–192) the majority of protein forms ring-shaped oligomers, and no larger particles were seen (Fig. 3). Even at increased concentrations (6 and 10 μM) RAD52-(1–192) shows no larger aggregates (data not shown). Higher magnifications reveal "protrusions" extending from the 10-nm rings formed by wild-type RAD52 that are missing in the 1–192 protein (see *arrows* in Fig. 3, *B* and *D*). These protrusions likely correspond to those modeled by Stasiak *et al.* (21), and our data show that they are part of the C-terminal portion of RAD52.

STEM analyses of wild-type RAD52 (2 μM) showed particle sizes ranging from 175 to 625 kDa with a mass average of 298 ± 69 kDa (n = 309; Fig. 4*A*). Given a molecular mass of 48 kDa for the His-tagged RAD52 protein, this range corresponds to particles that contain from 4 to 13 subunits with an average of six subunits. Similar analyses of the 1–192 protein showed particle sizes ranging from 100 to 350 kDa with a mass average of 227 ± 30 kDa (n = 277; Fig. 4*B*). For a monomer molecular mass of 23 kDa, this range corresponds to particles that contain from 4 to 15 subunits with an average of 10 subunits. Resolution of the ring-shaped oligomers in the electron micrographs was not high enough to count individual subunits, but our STEM data are consistent with previous work in which oligomeric rings of wild-type RAD52 were determined to be heptameric (21).

The oligomeric distribution of these proteins in solution was investigated by DLS. Wild-type RAD52 shows a multimodal profile with three peaks corresponding to particles with an average hydrodynamic radius of 6.6, 27.6, and 711.0 nm, respectively (Table I). These likely correspond to ring-shaped oligomers, the 30-nm particles described previously as "superrings" (12) and seen in our micrographs (Fig. 2), and larger aggregates also observed in our micrographs. We find that the percent distribution of these various sized particles is effected by protein concentration, *i.e.* with increasing concentration the larger aggregates account for a larger percentage of the population. In contrast to wild type, RAD52-(1–192) shows a monomodal light-scattering profile that corresponds to a particle with a hydrodynamic radius of 6.1 nm (Table I), which is in agreement with our EM analysis.

The above analyses indicate at least two modes of RAD52 self-association that are experimentally separable, (i) formation of ring-shaped oligomers and (ii) formation of larger aggregates. Because the latter seems to depend largely on the presence of residues C-terminal to position 192, we performed a number of assays to test for self-association on a mutant RAD52 containing only residues 218–418. Initial EM studies showed no distinct structural characteristics for this protein (data not shown), but STEM analysis revealed particle sizes ranging from 75 to 275 kDa (Fig. 4*C*) with a mass average of 153 ± 40 kDa (n = 119; Fig. 4*C*). Given a monomer molecular mass of 39 kDa, the particle composition ranges from two to seven subunits with an average of four subunits. Gel filtration shows a homogeneous peak corresponding to a molecular mass of 166 kDa (Fig. 5) and therefore to a particle containing approximately four subunits. Analysis by DLS shows a monomodal peak corresponding to a particle with an average R_H of 4.6 nm and a molecular mass of 118 kDa (therefore containing approximately three subunits). DLS measurements on thioredoxin alone show that it does not contribute to the oligomeric character of thioredoxin-RAD52-(218–418) (Table I). Together,

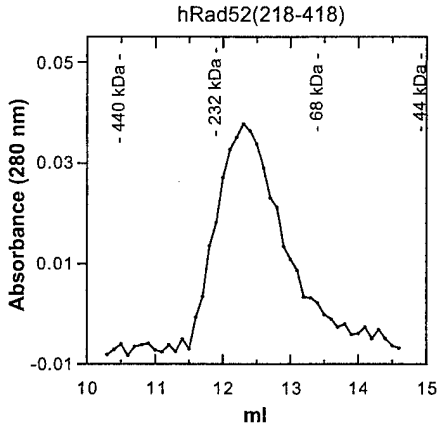

FIG. 5. **Gel filtration profile of the thioredoxin/218–418 fusion RAD52 protein.** The mutant protein (1.2 mg/ml, 35.8 μM) was loaded onto a Superdex 200 HR 10/30 gel filtration column, and elution of protein was followed at $A_{280\ nm}$. The indicated elution volumes of standards (ferritin, *440 kDa*; catalase, *232 kDa*; BSA, *68 kDa*; ovalbumin, *44 kDa*) were an average of four runs.

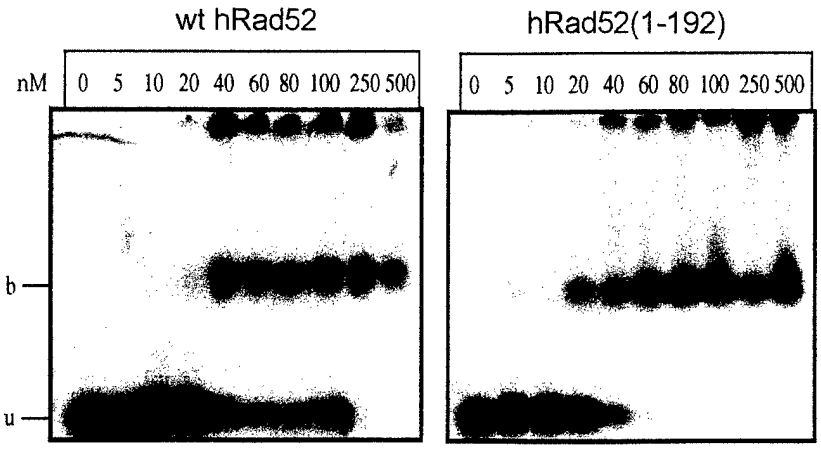

FIG. 6. **Gel-shift DNA Binding assays.** Indicated concentrations of either wild-type RAD52 or RAD52-(1–192) were incubated with a 5′-end-labeled 95-base oligonucleotide followed by cross-linking with glutaraldehyde as described under "Experimental Procedures." Reactions were electrophoresed on a 0.8% agarose gel. Radioactive material at the *top* of the gel represents protein-DNA complex trapped in the gel well. *u*, unbound DNA; *b*, protein-DNA complex.

these data indicate that the C-terminal portion of RAD52 (residues 218–418) contains determinants of protein self-association that are distinct from those required to form 10-nm rings.

DNA Binding—Binding of wild-type RAD52 and RAD52-(1–192) to single-stranded DNA was analyzed by gel-shift assays. The gels in Fig. 6 are representative of five different experiments, each of which gave similar results. In each case, analysis of unbound and bound DNA (including that in the gel well) gave rise to a $K_{D(app)}$ of 35 and 25 nM for wild-type RAD52 and RAD52-(1–192), respectively. This slight enhancement in binding affinity was observed consistently for RAD52-(1–192). With wild-type RAD52 a significant portion of bound DNA remained in the gel well, a result that likely reflects the ability of the wild-type protein to form greater amounts of self-aggregates than the 1–192 mutant protein (see below). Additionally, 100% of the DNA (2 nM total nucleotides) was bound by the 1–192 protein at 40–60 nM protein in the titration profile, whereas 100% binding by wild-type RAD52 consistently required greater than 100 nM protein. Assays using the RAD52-(218–418) mutant protein showed no DNA binding up to 2.0 μM protein (data not shown). These results show that the DNA binding domain of RAD52 is contained within the N-terminal portion of the protein and that removal of the C-terminal 227 residues results in a slight enhancement of DNA binding.

Interaction of RAD52 Proteins with RPA—Previous studies have mapped residues 221–280 as the domain in RAD52 that interacts with the 32-kDa subunit of RPA (16). To ensure that the 218–418 mutant construct maintained a native fold, we tested this protein for interaction with RPA using an immunoassay. Enzyme-linked immunosorbent assays showed that the 218–418 protein interacted with RPA with an affinity similar to that observed for wild-type RAD52 (Fig. 7). No interaction with RPA was observed for RAD52-(1–192), thioredoxin, or BSA.

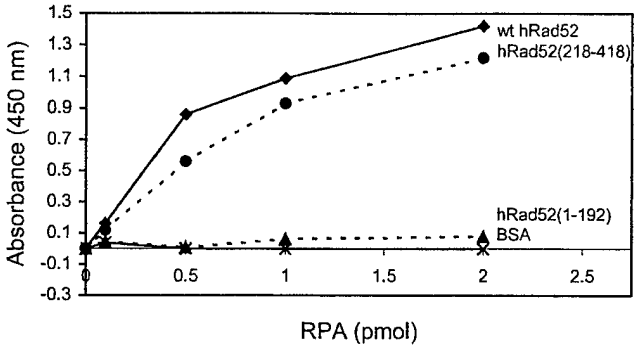

FIG. 7. **RAD52-RPA protein-protein interactions.** Enzyme-linked immunosorbent assays were performed as described under "Experimental Procedures" with RAD52 proteins immobilized to microtiter plates and probed with increasing amounts of RPA heterotrimer. The experiment was performed in triplicate, and the average for each RPA concentration was plotted. The error was on the order of 5–10%. *wt*, wild type.

DISCUSSION

Previous studies have shown that RAD52 exists in a number of oligomeric states ranging from rings with a 10-nm diameter to larger complexes with diameters of greater than 30 nm (9, 12, 20, 21). Recent observations indicate a direct role for these higher order protein-protein interactions in promoting DNA end-joining (20). We therefore sought to investigate the self-association properties of RAD52 utilizing an array of biophysical techniques.

In our EM studies of wild-type RAD52 and RAD52-(1–192), we observed ring structures with an average diameter of 10 ± 1 nm as has been reported previously (9, 12, 20, 21). Additionally, and as seen previously (12, 20, 21), we observed protrusions extending from wild-type RAD52 rings as well as a population of distinct larger particles. However, neither the protrusions nor the larger particles were observed with RAD52-(1–192). This suggests that residues within the C-terminal portion of the protein (residues 193–418) make up these protrusions and carry determinants for higher order RAD52 self-association.

DLS analysis of wild-type RAD52 and the two mutant proteins provides additional and complementary evidence for two distinct modes of RAD52 self-association. DLS analysis of wild-type RAD52 shows three peaks that likely correspond to the 10-nm ring-shaped oligomers and the 30-nm and larger particles observed by EM. In contrast, both RAD52-(1–192) and RAD52-(218–418) show a monomodal DLS profile indicating the presence of a single population of structures. The RAD52-(1–192) R_H is consistent with a ring structure, and the RAD52-(218–418) R_H indicates a complex composed of three subunits. This self-association of RAD52-(218–418) was confirmed by size-exclusion chromatography and STEM.

The ability of RAD52-(218–418) to self-associate was unexpected. Previous studies have suggested that residues 65–165 define the exclusive self-association domain in the RAD52 protein (18). Shen *et al.* (18) found that although N-terminal fragments of the protein self-associated in two-hybrid screens and affinity chromatography assays, fragments containing various portions of the C terminus, *e.g.* 287–418 or 166–418, did not. In contrast to these results, we find that RAD52-(218–418) is able to self-associate. Although our EM analysis revealed no distinct oligomeric structures for RAD52-(218–418), three different methods (STEM, gel filtration, and DLS) showed that this mutant formed oligomeric particles containing 3–4 subunits. These data for RAD52-(218–418), coupled with the inability of RAD52-(1–192) to form structures larger than the 10-nm rings, indicate that residues within the C-terminal region of the pro-

tein make important contributions to RAD52 self-association. Thus, the C-terminal region of RAD52 contains a novel self-association domain distinct from that previously identified within residues 65–165 (18).

Importantly, functional analyses of both the 1–192 and 218–418 mutant proteins show that each maintains an expected activity. Both wild-type RAD52 and the 1–192 proteins, which form ring-shaped oligomers, bound single-stranded DNA with similar affinities. This is consistent with previous studies that mapped the DNA binding domain of RAD52 to residues 39–80[2] (16). The elevated affinity of RAD52-(1–192) for single-stranded DNA was noted also for a similar Rad52p construct (24). Also as expected, RAD52-(218–418) showed a specific interaction with RPA. Again, this is consistent with previous studies that mapped the RPA interaction domain to residues 221–280 in RAD52 (16). The fact that both mutant proteins showed the expected functions demonstrates that they very likely maintain native structure, thereby supporting the relevance of differences observed in their oligomeric characteristics compared with wild-type RAD52.

In summary, our data support a model in which the self-association domain within the N-terminal region of RAD52 (residues 1–192) promotes the formation of ring-shaped oligomers that are functional for DNA binding, whereas the C-terminal domain (residues 218–418) mediates higher order self-association events. Additionally, the protrusions extending from the 10-nm ring structure of wild-type RAD52, originally modeled by Stasiak *et al.* (21) and seen clearly in our electron micrographs, correspond to the C-terminal region of the protein. Given the likely importance of higher order self-association to the ability of RAD52 to promote end-to-end joining of DNA breaks (20), these protrusions seem to mediate a critically important aspect of RAD52 function. Further studies of various mutant RAD52 proteins will clarify the contribution made by the different aspects of self-association toward the overall function of this important DNA repair protein.

Acknowledgments—We thank Matt Pokross and Jeff Habel for technical assistance and Krishnamurthy Rajeswari and Cathy Schellert for help in the early stages of this project. We also thank Dr. Min Park at Los Alamos National Laboratory for wild-type *RAD52* and *RAD52*-(1–192) expression plasmids. We gratefully acknowledge Dr. Martha Simon at Brookhaven National Laboratory for performing the STEM analyses.

REFERENCES

1. Game, J., and Mortimer, R. K. (1974) *Mutat. Res.* **24,** 281–292
2. Petes, T. D., Malone, R. E., and Symington, L. S. (1991) in *The Molecular and Cellular Biology of the Yeast, Saccharomyces* (Broach, J. R., Pringle, J. R., and Jones, E. W., eds) pp. 407–522, Cold Spring Harbor Laboratory Press, Cold Spring Harbor, NY
3. Shinohara, A., and Ogawa, T. (1998) *Nature* **391,** 404–407
4. Milne, G. T., and Weaver, D. T. (1993) *Genes Dev.* **7,** 1755–1765
5. Hays, S. L., Firmenich, A. A., and Berg, P. (1995) *Proc. Natl. Acad. Sci., U. S. A.* **92,** 6925–6929
6. Johnson, R. D., and Symington, L. S. (1995) *Mol. Cell. Biol.* **15,** 4843–4850
7. Sung, P. (1997) *J. Biol. Chem.* **272,** 28194–28197
8. New, J. H., Sugiyama, T., Zaitseva, E., and Kowalczykowski, S. C. (1998) *Nature* **391,** 407–410
9. Shinohara, A., Shinohara, M., Ohta, T., Matsuda, S., and Ogawa, T. (1998) *Genes Cells* **3,** 145–156
10. Sugiyama, T., New, J. H., and Kowalczykowski, S. C. (1998) *Proc. Natl. Acad. Sci. U. S. A.* **95,** 6049–6054
11. Wold, M. S. (1997) *Annu. Rev. Biochem.* **66,** 61–91
12. Van Dyck, E., Hajibagheri, N. M. A., Stasiak, A., and West, S. C. (1998) *J. Mol. Biol.* **284,** 1027–1038
13. Golub, E. I., Gupta, R. C., Haaf, T., Wold, M. S., and Radding, C. M. (1998) *Nucleic Acids Res.* **26,** 5388–5393
14. Baumann, P., and West, S. C. (1999) *J. Mol. Biol.* **291,** 363–374
15. Shen, Z., Cloud, K. G., Chen, D. J., and Park, M. S. (1996) *J. Biol. Chem.* **271,** 148–152
16. Park, M. S., Ludwig, D. L., Stigger, E., and Lee, S. H. (1996) *J. Biol. Chem.* **271,** 18996–19000
17. Benson, F. E., Baumann, P., and West, S. C. (1998) *Nature* **391,** 401–404
18. Shen, Z., Peterson, S. R., Comeaux, J. C., Zastrow, D., Moyzis, R. K., Bradbury, E. M., and Chen, D. J. (1996) *Mutat. Res.* **364,** 81–89
19. Kito, K., Wada, H., Yeh, E. T., and Kamitani, T. (1999) *Biochim. Biophys. Acta* **1489,** 303–314
20. Van Dyck, E., Stasiak, A. Z., Stasiak, A., and West, S. C. (1999) *Nature* **398,** 728–731
21. Stasiak, A. Z., Larquet, E., Stasiak, A., Muller, S., Engel, A., Dyck, E. V., West, S. C., and Egelman, E. H. (2000) *Curr. Biol.* **10,** 337–340
22. Henricksen, L. A., Umbricht, C. B., and Wold, M. S. (1994) *J. Biol. Chem.* **269,** 11121–11132
23. Wall, J. S., Hainfeld, J. F., and Simon, M. N. (1998) *Methods Cell Biol.* **53,** 139–164
24. Mortensen, U. H., Bendixen, C., Sunjevaric, I., and Rothstein, R. (1996) *Proc. Natl. Acad. Sci. U. S. A.* **93,** 10729–10734

BATCH: bi7e19 USER: dge69 DIV: @xyv04/data1/CLS_pj/GRP_bi/JOB_i30/DIV_bi0155089 DATE: June 8, 2001

Human RAD52 Protein Has Extreme Thermal Stability†

Wasantha Ranatunga, Doba Jackson, Robert A. Flowers II, and Gloria E. O. Borgstahl*

Department of Chemistry, The University of Toledo, Toledo, Ohio 43606-3390

Received February 2, 2001; Revised Manuscript Received April 27, 2001

ABSTRACT: The human RAD52 protein plays an important role in the earliest stages of chromosomal double-strand break repair via the homologous recombination pathway. Individual subunits of RAD52 associate into seven-membered rings. These rings can form higher order complexes. RAD52 binds to DNA breaks, and recent studies suggest that the higher order self-association of the rings promotes DNA end joining. Monomers of the RAD52(1−192) deletion mutant also associate into ring structures but do not form higher order complexes. The thermal stability of wild-type and mutant RAD52 was studied by differential scanning calorimetry. Three thermal transitions (labeled A, B, and C) were observed with melting temperatures of 38.8, 73.1, and 115.2 °C. The RAD52(1−192) mutant had only two thermal transitions at 47.6 and 100.9 °C (labeled B and C). Transitions were labeled such that transition C corresponds to complete unfolding of the protein. The effect of temperature and protein concentration on RAD52 self-association was analyzed by dynamic light scattering. From these data a four-state hypothetical model was developed to explain the thermal denaturation profile of wild-type RAD52. The three thermal transitions in this model were assigned as follows. Transition A was attributed to the disruption of higher order assemblies of RAD52 rings, transition B to the disruption of rings to individual subunits, and transition C to complete unfolding. The ring-shaped quaternary structure of RAD52 and the formation of higher ordered complexes of rings appear to contribute to the extreme stability of RAD52. Higher ordered complexes of rings are stable at physiological temperatures in vitro.

RAD52[1] protein plays a critical role in mitotic and meiotic recombination as well as double-strand break repair (*1*, *2*). On the basis of a series of protein−protein interaction assays and DNA binding studies (*3*−*5*), a domain map of human RAD52 (RAD52) was proposed by Park et al. (Figure 1). Electron microscopy (EM) studies of *Saccharomyces cerevisiae* and human RAD52 have revealed formation of ring-shaped structures (9−13 nm in diameter), as well as higher order aggregates (*6*−*8*). The RAD52 rings appear to be composed of seven subunits (*9*). EM studies also showed that RAD52 recognizes and binds to double-stranded DNA ends as an aggregated complex that ranges in size from approximately 15 to 60 nm in diameter (*8*). This binding promoted end-to-end association between DNA molecules and stimulated the ligation of both cohesive and blunt DNA ends (*8*). Recently, by studying wild type and two deletion mutants of RAD52 (Figure 1), we demonstrated that the self-association domain in the N-terminal half of RAD52 is responsible for ring formation and that elements in the C-terminal half of the molecule participate in the formation of higher order complexes of rings (*10*).

Due to the biological interest of human RAD52 and the apparent biochemical importance of RAD52 self-association in DNA repair, we studied its multiple levels of self-association and stability using biophysical methods. The stability of wild-type RAD52 was studied by differential scanning calorimetry (DSC). To investigate the basis for the extreme stability of RAD52 that was discovered, two mutants were also studied, RAD52(1−192) and RAD52(218−418) (Figure 1). The effects of temperature and protein concentration on the hydrodynamic radius (R_H) of RAD52 were studied by dynamic light scattering (DLS). Finally, a hypothetical model of the effects of protein aggregation state on thermal stability was developed.

MATERIALS AND METHODS

Protein Purification. The domain structures for wild-type RAD52, RAD52(1−192), and RAD52(218−418) are described in Figure 1. Proteins were expressed, purified under reducing conditions, and concentrated as described (*10*). Unfortunately, enterokinase cleavage was nonspecific, and the histidine-patch thioredoxin (Invitrogen) could not be separated from the 218−418 peptide (Jackson, unpublished results). After the extreme thermal stability of wild-type RAD52 was observed, subsequent purifications included a heat treatment step. The lysate was heated to 55 °C for 30 min prior to the chromatography steps. Samples were concentrated using an Ultrafree-15 centrifugal filter device. After each step of concentration, the samples were analyzed by DLS. Protein concentrations were determined using the Bradford assay (Bio-Rad) with bovine serum albumin as a standard.

Differential Scanning Calorimetry. Protein and reference solutions were degassed under a vacuum for 15 min before

† This work was supported by the U.S. Army Medical Research and Material Command under DAMD17-98-1-8251.

* To whom correspondence should be addressed. Telephone: 419-530-1501. Fax: 419-530-4033. E-mail: gborgst@uoft02.utoledo.edu.

[1] Abbreviations: RAD52, human RAD52; DLS, dynamic light scattering; DSC, differential scanning calorimetry; EM, electron microscopy; MnSOD, manganese superoxide dismutase; SOS, sum of squares; R_H, hydrodynamic radius; T_M, melting temperature.

10.1021/bi0155089 CCC: $20.00
Published on Web 00/00/0000 PAGE EST: 5.6

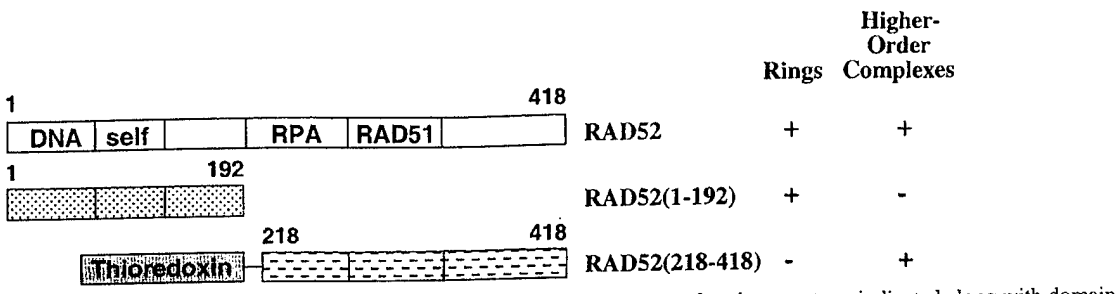

FIGURE 1: Wild-type RAD52 and deletion mutants. Beginning and ending residue numbers of each mutant are indicated along with domain structure. The following domains and residue numbers were defined by Park et al. (*16*): DNA binding (39−80), self-association (85−159), RPA binding (221−280), and RAD51 binding (290−330). The structural characterization of wild-type and mutant RAD52 by Ranatunga et al. is summarized on the right (*10*). Wild-type RAD52 and RAD51(1−192) have six histidines fused to the C-terminus. For the RAD52-(218−418) mutant, a thrombin-cleavable six-histidine tag is fused to the N-terminus of the histidine-patch thioredoxin, and an enterokinase cleavage site separates histidine-patch thioredoxin from RAD52(218−418).

data acquisition. The concentration of wild-type RAD52 was 2.0 and 3.5 mg/mL, RAD52(1−192) was 7.2 mg/mL, and RAD52(218−418) was 3.1 mg/mL. The wild-type RAD52 sample was concentrated to 11.5 mg/mL before dilution to either 2.0 or 3.5 mg/mL. The concentrations of wild-type RAD52 and RAD52(218−418) were limited by the quantity of protein available. The protein samples and reference solutions were loaded into their respective cells in the MicroCal MC-2 differential scanning calorimeter. An external pressure of 30 psi was applied with nitrogen gas to both sample and reference cells. The sample was scanned relative to the reference solution over a temperature range of 5−120 °C at a rate of 45 °C/h. DSC measurements on buffer alone had no transitions for the temperature range 5−120 °C. The baseline and change in specific heat (ΔC_p) upon denaturation were corrected according to standard techniques (*11*). DSC data were fit to a two- or three-state model using the Origin DSC software provided by Microcal Inc.

Dynamic Light Scattering Analysis. DLS was carried out using a DynaPro-801 molecular sizing instrument equipped with a temperature-controlled microsampler (Protein Solutions). A 50 μL sample was passed through a filtering assembly equipped with a 100 nm filter into a 12 μL chamber quartz cuvette. For each experiment, 35−60 measurements were taken. The data were first analyzed using Dynamics 4.0 software and then with DynaLS software. The refractive index and viscosity of the buffer at each temperature were measured and the proper corrections applied to the data. Baseline and sum of squares (SOS) error values were reported by Dynamics 4.0. The baseline is the measured value of the last coefficient in the correlation curve. Baselines within the range from 0.977 to 1.002 were interpreted as monomodal, and those greater than 1.002 were bi- or multimodal. The SOS error is the sum of squares difference between the measured correlation curve and the best-fit curve. SOS errors less than 5.000 were considered negligible. Errors between 5.000 and 20.000 were considered as low and probably due to low protein concentration or a small amount of polydispersity. Errors greater than 20.000 were considered as high and are probably due to high polydispersity in size distribution (aggregation) or irregular solvent. Mean R_H, standard deviation, and percent of peak area are reported from DynaLS using the optimized resolution. Due to the irregular solvent, the SOS errors increased for diluted samples, and it was necessary to use DynaLS to separate the solvent peak from the protein peak.

RESULTS AND DISCUSSION

Differential Scanning Calorimetry. Thermal stability profiles of wild-type RAD52, RAD52(1−192), and RAD52-(218−418) were obtained by DSC (Figure 2 and Table 1). For wild-type RAD52 and RAD52(1−192) the DSC transitions were labeled A, B, or C such that total unfolding was always labeled C. For wild-type RAD52, at 2.0 mg/mL, the DSC profile was composed of two transitions (labeled B and C) with melting temperatures (T_M) of 78.3 and 101.6 °C (Table 1). At 3.5 mg/mL, the wild-type RAD52 DSC profile was composed of three distinct transitions (labeled A, B, and C in Figure 2A) with T_M's of 38.8, 73.1, and 115.2 °C (Table 1). When the concentration of wild-type RAD52 was increased, transition C was shifted to a higher temperature by 13 °C. Transition A could be measured only if the sample was first concentrated to 11.5 mg/mL and then diluted to 3.5 mg/mL. For RAD52(1−192) two transitions were observed at 47.6 and 100.9 °C (labeled B and C in Figure 2B). The deletion of the C-terminal half of RAD52 decreased the T_M of transitions B and C by 25 and 14 °C, respectively.

Our earlier analysis demonstrated that wild-type RAD52 forms ring structures as well as higher order complexes of rings but RAD52(1−192) forms rings but not the aggregates of rings (*10*). The size of the wild-type RAD52 higher order complexes, as well as the proportion of the rings in a higher order complex, is dependent on concentration. RAD52(1−192) rings do not form higher ordered complexes, at any concentration. DSC transition A was dependent on the concentration of wild-type RAD52 and was not observed for RAD52(1−192). Therefore, it appeared that transition A corresponded to the thermal disruption of aggregates to form single rings in solution, transition B to the break up of rings to monomers, and transition C to the total unfolding of monomers.

The DSC profile of RAD52(218−418) is also consistent with this interpretation (Figure 2C). RAD52(218−418) forms a complex of two to four monomers depending on the concentration but does not form ring structures in solution (*10*). It has a relatively low T_M of 53−59 °C, and it appears that the C-terminal half of RAD52, which cannot form rings, is not as thermally stable as the ring-structured N-terminal half.

Wild-type *Escherichia coli* thioredoxin is a very stable protein with a T_M of ~85 °C for the oxidized form and ~73

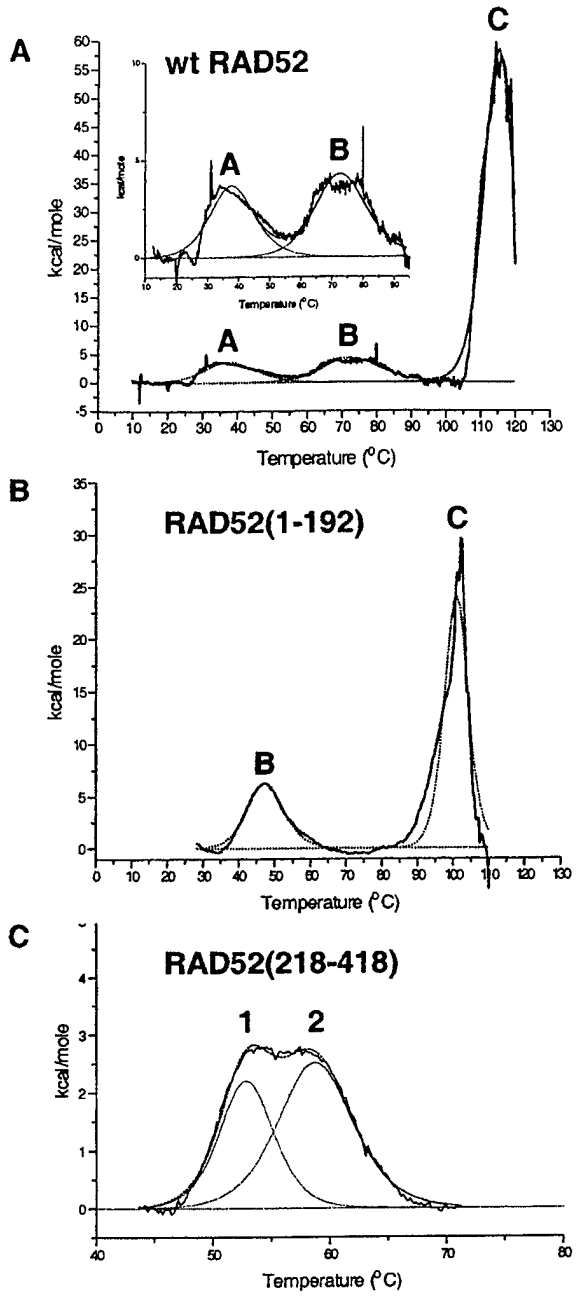

FIGURE 2: Thermal stability of wild-type RAD52 and deletion mutants. DSC profiles for (A) wild-type RAD52 were analyzed at 0.038 mM (3.5 mg/mL), (B) RAD52(1−192) at 0.325 mM (7.2 mg/mL), and (C) RAD52(218−418) at 0.082 mM (3.1 mg/mL). For RAD52(218−418) there were no transitions above 70 °C.

°C for the reduced form (*12*, *13*). When thioredoxin is fused to other proteins, it can improve their solubility and, especially when in the oxidized form, improve their thermal stability, allowing a heat step during purification. Histidine-patch thioredoxin in the reduced state was expected to have a T_M of ~67 °C (*12*−*14*). We were unable to specifically cleave thioredoxin from RAD52(218−418) with enterokinase, so the exact contributions of thioredoxin and RAD52-(218−418) to the DSC profile of the fusion protein could not be determined. It is apparent that fusing thioredoxin to RAD52(218−418) has reduced the T_M of thioredoxin significantly and that RAD52(218−418) by itself would probably have a T_M lower than that measured for the fusion protein.

Table 1: Thermodynamic Parameters from DSC Measurement of RAD52 Proteins

protein	concn (mg/mL)	component	T_M (°C)
RAD52[a]	2.0	B	78.3
		C	101.6
RAD52[b]	3.5	A	38.8
		B	73.1
		C	115.2
RAD52(1−192)[c]	7.2	B	47.6
		C	100.9
RAD52(218−418)[d]	3.1	1	53.4
		2	59.1

[a] This sample was concentrated to 11.5 mg/mL and then diluted to 2.0 mg/mL (similar to Table 2, line 12) and does not contain higher ordered assemblies of rings. [b] This sample was concentrated to 11.5 mg/mL and then diluted to 3.5 mg/mL for DSC measurements (similar to Table 2, line 7, and Figure 3E) and contains higher ordered complexes of rings. [c] RAD52(1−192) forms rings but does not form higher ordered assemblies of rings (*10*). [d] RAD52(218−418) does not form rings but does self-associate (*10*).

The reversibility of transitions A, B, and C for wild-type RAD52 was studied by DSC, using an 11.5 mg/mL sample diluted to 3.5 mg/mL. Three experiments were performed, and the presence of precipitation was noted after each (data not shown). First, the sample was heated to 55 °C and then slowly returned to 20 °C overnight. Transition A was observed, and the protein remained in solution. Then the same sample was heated to 95 °C and slowly returned to 20 °C overnight. During this second experiment, transition A did not return, possibly due to the protein concentration used (see discussion of DLS data, Table 2, lines 7−9), and transition B was lowered to 65 °C. After the second experiment there was a slight amount of precipitate, but the majority of the protein was still in solution. For the third experiment, the sample was heated to 120 °C, and there was only one significant peak at 94 °C and the protein completely precipitated. The T_M for complete unfolding was lower than that measured from fresh sample (115 °C for peak C, Figure 2A), indicating that the protein did not properly reassemble after the second experiment and that the process of unfolding is irreversible under this set of experimental conditions.

The irreversibility of transition B was also noted in experiments performed during the addition of a heat step to the purification protocol for wild-type RAD52. Lysates were heated in 5 deg increments between 55 and 80 °C, centrifuged, and analyzed by SDS−PAGE. RAD52 began to precipitate after 65 °C (data not shown). This supports the conclusion that transition B in the thermal denaturation of RAD52 is irreversible.

Dynamic Light Scattering. The response of RAD52 rings and higher ordered complexes to concentration and temperature was studied by DLS. The upper temperature limit of the DLS microsampler was 50 °C so theoretically data on transition A of wild-type RAD52 and transition B of RAD52-(1−192) could be measured.

The procedure followed for sample preparation affected the detection of DSC transition A and the T_M value of transition C for wild-type RAD52, so the effects of protein concentration and temperature on the R_H of wild-type RAD52 were studied using DLS. In a series of experiments, the protein concentration was increased from 3.5 to 11.5 mg/

Table 2: Effect of Temperature and Concentration on R_H of Wild-Type RAD52

DLS expt	concn (mg/mL)	base-line	SOS error[a]	R_H[b] (nm)	peak area[c] (%)	interpre-tation[d]
1. 20 °C	3.5	1.001	4.22	**15.0 (2.5)**	**98.3**	>2 rings
2. heat to 50 °C	3.5	1.000	2.78	**14.2 (4.5)**	**99.2**	~2 rings
3. concd; 20 °C	4.9	1.002	2.03	4.3 (0.5)	3.4	monomer
				18.7 (2.3)	**95.8**	>2 rings
4. concd; 20 °C	11.5	1.009	7.78	5.1 (0.6)	4.2	mono/ dimer
				17.8 (3.1)	**56.9**	>2 rings
				36.1 (4.4)	**36.6**	≫2 rings
5. heat to 50 °C	11.5	1.000	5.96	**19.2 (8.5)**	**99.2**	>2 rings
6. cool to 20 °C	11.5	1.010	8.24	5.9 (0.4)	9.7	mono/ dimer
				11.2 (0.7)	6.6	1−2 rings
				20.6 (2.2)	**81.6**	>2 rings
7. sample from line 4 diluted; 20 °C	3.5	1.001	11.3	3.8 (0.2)	0.6	monomer
				23.2 (11.6)	**98.1**	>2 rings
8. heat to 50 °C	3.5	1.001	9.41	**9.7 (1.2)**	**45.8**	1 ring
				17.0 (1.0)	**49.8**	>2 rings
9. cool to 20 °C	3.5	1.001	16.1	3.9 (0.2)	1.1	monomer
				11.9 (1.9)	**69.3**	1−2 rings
				28.6 (3.5)	**26.4**	≫2 rings
10. sample from line 3 diluted; 20 °C	3.3	1.001	7.4	**3.1 (0.2)**	**11.0**	monomer
				16.8 (5.4)	**84.0**	>2 rings
				49.5 (8.7)	**14.5**	≫2 rings
11. heat to 37 °C	3.3	1.000	7.9	**19.8 (10.9)**	**99.5**	>2 rings
12. sample from line 4 diluted; 20 °C	2.3	1.001	50.9	**8.75 (6.0)**	**79.7**	1 ring
13. heat to 37 °C	2.3	1.000	24.5	**8.0 (1.6)**	**71.9**	1 ring
14. heat to 50 °C	2.3	1.000	15.9	**8.7 (2.7)**	**87.4**	1 ring

[a] SOS = sum of squares. [b] Average R_H is given with the standard deviation given in parentheses. [c] DynaLS results; the percent peak area for the solvent peaks was not reported. DLS measurements at 20 and 50 °C on solvent alone indicate that very small and very large components in the RAD52 measurements were due to the solvent and not the protein. Therefore, only the peaks attributable to RAD52 protein are reported (R_H > 3.0 nm; see Figure 4). R_H and percent peak area of the primary species in solution (greater than 10%) are in bold. [d] Interpretation is based on estimated R_H in Figure 4. It is not possible to tell exactly how many rings of RAD52 are in the aggregates >14.1 nm since the structure of the higher order complexes of RAD52 rings is unknown.

mL and then diluted (see Table 2 and Figure 3). The microsampler cell was held at 20, 37, or 50 °C, and samples were equilibrated for 30 min at the target temperature before DLS measurements began. The smallest R_H measured for RAD52 was 8.0−8.75 nm (Table 2, lines 12−14). This is close to the size expected for single rings measured from electron micrographs (Figure 4) (*6*−*8*). A monomer of RAD52 is expected to have an R_H value of 3.2 nm, and complexes containing two rings are expected to have an R_H of 12.8−14.1 nm. The R_H for aggregates of more than two rings would be greater than 14 nm.

Using these estimates of particle sizes as a guide, four trends in the DLS data were noted. First, heating the protein samples from 20 to 50 °C caused the R_H to decrease in general, and frequently the baseline decreased to within the monomodal range. For example, heating a sample similar to that used for DSC measurements (Table 2, line 7, and Figure 3E) caused the particles to shift from a single population with R_H of 23.2 nm to two populations with R_H of 9.7 and 17.0 nm (Table 2, line 8, and Figure 3F). Second, the size of the sample population was dependent on the protein concentration. For example, the R_H of the sample

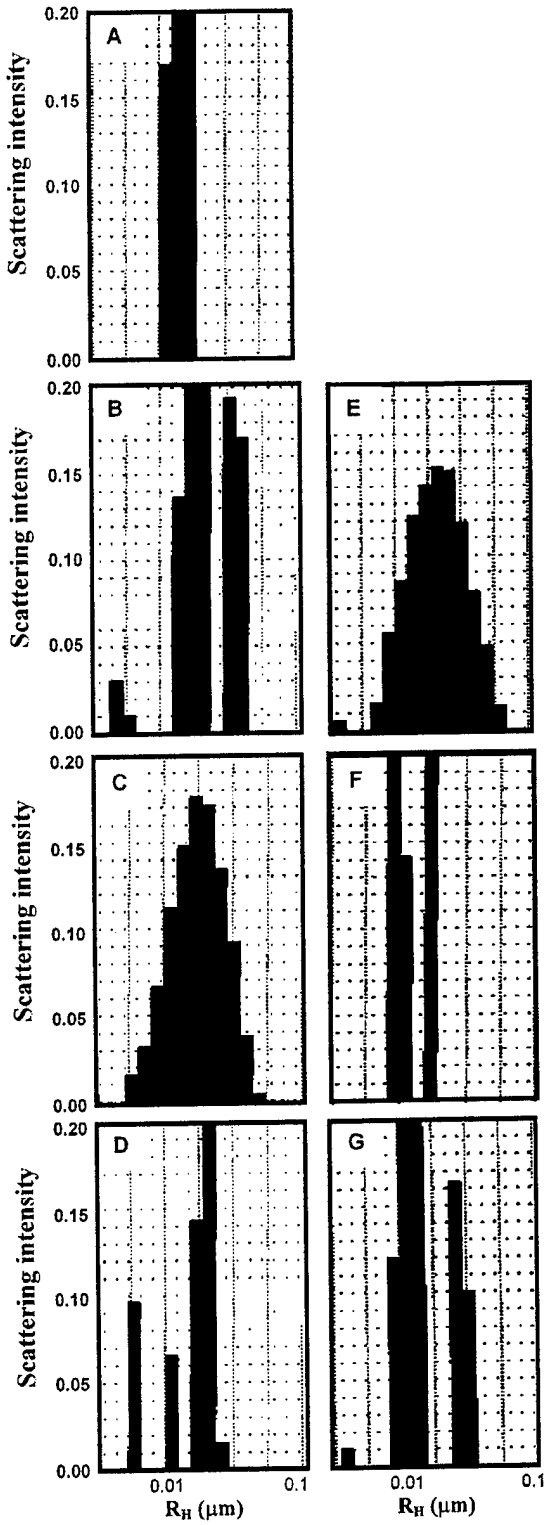

FIGURE 3: Effect of protein concentration and temperature on the R_H of wild-type RAD52. DLS data were analyzed using DynaLS software. The data correspond to the following lines in Table 2: (A) 3.5 mg/mL at 20 °C (line 1), (B) 11.5 mg/mL at 20 °C (line 4), (C) 11.5 mg/mL at 50 °C (line 5), (D) 11.5 mg/mL cooled to 20 °C (line 6), (E) diluted to 3.5 mg/mL at 20 °C (line 7), (F) diluted to 3.5 mg/mL at 50 °C (line 8), and (G) diluted to 3.5 mg/mL cooled to 20 °C (line 9). Panels E−G correspond to the sample used for DSC.

Model	R_H (nm)
Monomer	3.2
7-membered ring	8.5
Two edge on rings	14.1
Two stacked rings	12.8

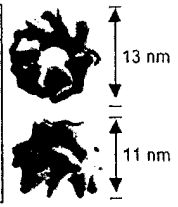

FIGURE 4: Estimated R_H for RAD52 models. The R_H for a monomer was calculated from a molecular mass of 47.0 kDa with the molecular weight calculator included in the Dynamics 3.0 software. R_H for a seven-membered ring of RAD52 was estimated from the diagonal of the three-dimensional reconstruction on the basis of electron micrographs (*9*). Electron micrographs of RAD52 rings in the large, greater than 100 nm spherical aggregates appear to have an "edge-on" orientation (*10*). The three-dimensional reconstructions of RAD52 were adapted from Stasiak et al. (2000).

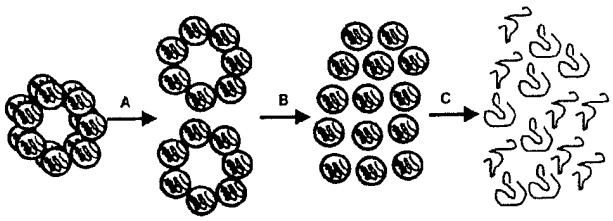

FIGURE 5: Hypothetical four- state model for the thermal denaturation of wild-type RAD52. Transitions A, B, and C correspond to those measured by DSC in Figure 2. There are three transitions in this model; transition A is attributed to the disruption of higher order assemblies of RAD52 rings, transition B to the disruption of rings to individual subunits, and transition C to complete unfolding. The individual subunits after transition B are probably partially unfolded as well as disassociated from the rings.

population increased from 15.0 to 18.7 to 36.1 nm, when the concentration was increased from 3.5 to 4.9 to 11.5 mg/mL (Table 2, lines 1, 3, and 4). Third, the modality of the sample population was dependent on the protein concentration. For example, the 11.5 mg/mL sample was multimodal at 20 °C (Table 2, line 4, and Figure 3B), and the 3.5 mg/mL sample was not (Table 2, line 1, and Figure 3A). Fourth, the reversibility of the assembly of RAD52 rings into higher ordered complexes was dependent on protein concentration. The majority of the particles in the samples at 11.5 mg/mL remained greater than 17 nm throughout the heat cycle (Table 2, lines 4−6, and Figure 3B−D). But, the superaggregation of rings was only partially reversible at 3.5 mg/mL with only 26% of the sample returning to greater than 17 nm after being heated (Table 2, lines 7−9, and Figure 3E−G). It is noteworthy that for the DSC measurements made on samples at 3.5 mg/mL the assembly of RAD52 rings into higher ordered complexes is not completely reversible at this concentration.

Finally, this DLS analysis facilitated the interpretation of DSC transition A. Transition A could not be detected for samples that were first concentrated to 11.5 mg/mL and then diluted to 2.0 mg/mL (prepared as in line 12, Table 2). The R_H value of 8.75 indicates that at 2.0 mg/mL there are primarily single rings in solution and little or no higher ordered complexes (Figure 4). Transition A was detectable for samples that were diluted to 3.5 mg/mL (prepared as in line 7, Table 2, and Figure 3E). The R_H value of 23.2 nm indicates that at 3.5 mg/mL there are primarily higher order complexes of many rings in solution. Heating this sample to 50 °C caused the R_H to decrease and form two populations of 9.7−17.0 nm (Table 2, line 8, and Figure 3F). Therefore, these DLS data indicate that DSC transition A can be attributed to the disassociation of rings from higher ordered complexes.

We were interested to know if the higher ordered complexes of RAD52 rings were stable at physiological temperatures. Protein samples diluted to 3.3 mg/mL did not form particles less than 9 nm upon heating to 37 °C (Table 2, lines 10 and 11) although the samples became monomodal. Therefore, the upper level aggregation of RAD52 rings is stable at physiological temperatures in vitro.

Transition B of the RAD52(1−192) mutant was 47.6 °C, and attempts were made to measure the effect of temperature on the structure of RAD52(1−192) with DLS. Higher ordered assemblies of rings are not formed by RAD52(1−192), and single rings have an R_H of 5.7 nm (SD = 1.2) (*10*). As samples of RAD52(1−192) were heated, the R_H appeared to increase, perhaps indicating partial unfolding (data not shown). DLS measurements at elevated temperatures with RAD52(1−192) were very problematic, and at 50 °C no measurements could be obtained, perhaps due to large changes in structure.

CONCLUSIONS

Our data indicate that the RAD52 rings and higher ordered complexes of rings used in DNA repair and DNA recombination are extremely stable structures. The structure of wild-type RAD52 is very stable, and its multiple levels of self-association appear to contribute to this stabilization. The extreme stability of the wild-type RAD52 and RAD52(1−192) folds relative to RAD52(218−418) appears to be related to the assembly of multiple monomers into a ring. The enhanced stability of the wild-type RAD52 fold relative to RAD52(1−192) appears to be due in part to its ability to form higher order assemblies of rings.

A four-state hypothetical model has been developed to explain the thermal denaturation profile of wild-type RAD52 (Figure 5). There are three transitions in this model; transition A is attributed to the disruption of higher order assemblies of RAD52 rings, transition B to the disruption of rings to individual subunits, and transition C to complete unfolding. Individual rings of RAD52 appear to have an R_H on the order of 8.0−8.75 nm in solution (Table 2, lines 12−14). Higher order assemblies of rings are seen in the wild-type RAD52 DLS data as particles ranging from 15 to 50 nm. Note that the measured R_H values are not integral values of individual rings due to the presence of equilibrium mixtures of single rings and complexes of rings in solution as indicated by the high standard deviations in the R_H measurements (Table 2) and the width of the DLS peaks (Figure 3). This equilibrium is dependent upon concentration. At concentrations of 3.5 mg/mL or greater RAD52 appears to be primarily composed of assemblies of two or more rings with R_H values ranging from 15 to 36.1 nm. Raising the temperature from 20 to 50 °C disrupts the higher order particles, pushing the equilibrium toward the 9 nm particles (Table 2, lines 5 and 8, and Figure 3C and F). These data support our hypothetical model for transition A (Figure 5). Reliable DLS measurements varying temperature on RAD52(1−192) could not be made. Thermal expansion of the RAD52(1−192) rings was noted. The data indicate that a large structural transition occurs near transition

B, possibly the disassociation of individual subunits from the rings.

Only a handful of proteins have been measured with thermal stabilities on the order of RAD52. To our knowledge, the highest T_M for a protein reported in the literature to date is 125 °C for ferredoxin from the hyperthermophile *Thermotoga maritima* (*15*). Other proteins such as onconase and mitochondrial manganese superoxide dismutase (MnSOD) are extremely stable with T_M's approaching 90 °C (*16*, *17*). Both ferredoxin and onconase are monomeric, and by studying their protein crystal structures, their stabilities were attributed to the compactness of their tertiary structures and to extensive hydrogen bonding involving charged amino acid side chains. Mitochondrial MnSOD is a homotetramer, and its enhanced stability was partially attributed to its quaternary structure. The DSC profile of MnSOD has three thermal transitions (labeled A, B, and C), similar to those seen with RAD52. Transition A was attributed to subunit disassociation, transition B to loss of the active site manganese, and transition C to complete unfolding. A cavity forming point mutation in the tetrameric interface of MnSOD resulted in the lowering of transition B by 13.6 °C and transition C by 16.5 °C (*17*). These results on MnSOD are somewhat similar to the results on RAD52. We conclude from our data that both components of RAD52 self-association, ring formation and higher order complex formation, contribute to its extreme thermal stability. A precise understanding of the structural determinants of RAD52 stability awaits the solution of its crystal structure.

ACKNOWLEDGMENT

We thank Dr. Min Park for providing the expression plasmid for RAD52(1−192).

REFERENCES

1. Game, J., and Mortimer, R. K. (1974) *Mutat. Res. 24*, 281−292.
2. Petes, T. D., Malone, R. E., and Symington, L. S. (1991) in *The Molecular and Cellular Biology of the Yeast, Saccharomyces* (Broach, J. R., Pringle, J. R., and Jones, E. W., Eds.) pp 407−522, Cold Spring Harbor Laboratory Press, Cold Spring Harbor, NY.
3. Shen, Z., Cloud, K. G., Chen, D. J., and Park, M. S. (1996) *J. Biol. Chem. 271*, 148−152.
4. Shen, Z., Peterson, S. R., Comeaux, J. C., Zastrow, D., Moyzis, R. K., Bradbury, E. M., and Chen, D. J. (1996) *Mutat. Res. 364*, 81−89.
5. Park, M. S., Ludwig, D. L., Stigger, E., and Lee, S. H. (1996) *J. Biol. Chem. 271*, 18996−19000.
6. Shinohara, A., Shinohara, M., Ohta, T., Matsuda, S., and Ogawa, T. (1998) *Genes Cells 3*, 145−156.
7. Van Dyck, E., Hajibagheri, N. M. A., Stasiak, A., and West, S. C. (1998) *J. Mol. Biol. 284*, 1027−1038.
8. Van Dyck, E., Stasiak, A. Z., Stasiak, A., and West, S. C. (1999) *Nature 398*, 728−731.
9. Stasiak, A. Z., Larquet, E., Stasiak, A., Muller, S., Engel, A., Dyck, E. V., West, S. C., and Egelman, E. H. (2000) *Curr. Biol. 10*, 337−340.
10. Ranatunga, W., Jackson, D., Lloyd, J. A., Forget, A. L., Knight, K. L., and Borgstahl, G. E. O. (2001) *J. Biol. Chem.* (in press).
11. Haynie, D. T., and Freire, E. (1994) *Anal. Biochem. 216*, 33−41.
12. Ladbury, J., Wynn, R., Hellinga, H., and Sturtevant, J. (1993) *Biochemistry 32*, 7526−7530.
13. Ladbury, J., Kishore, N., Hellinga, H., Wynn, R., and Sturtevant, J. (1994) *Biochemistry 33*, 3688−3692.
14. Lu, Z., DiBlasio-Smith, E., Grant, K., Warne, N., LaVallie, E., Collins-Racie, L., Follettie, M., Williamson, M., and McCoy, J. (1996) *J. Biol. Chem. 271*, 5059−5065.
15. Pfeil, W., Gesierich, U., Kleemann, G. R., and Sterner, R. (1997) *J. Mol. Biol. 272*, 591−596.
16. Notomista, E., Catanzano, F., Graziano, G., Piaz, F. D., Barone, G., D'Alessio, G., and Donato, A. D. (2000) *Biochemistry 39*, 8711−8718.
17. Borgstahl, G. E. O., Parge, H. E., Hickey, M. J., Johnson, M. J., Boissinot, M., Hallewell, R. A., Lepock, J. R., Cabelli, D. E., and Tainer, J. A. (1996) *Biochemistry 35*, 4287−4297.

BI0155089